Nanoscale

PAPER

Making biological membrane resistant to the toxicity of misfolded protein oligomers: a lesson from trodusquemine†

Silvia Errico,[a,b] Giacomo Lucchesi,[c] Davide Odino,[d] Stefano Muscat, [iD][e]
Claudia Capitini,[f,g] Chiara Bugelli,[a] Claudio Canale,[d] Riccardo Ferrando, [iD][d]
Gianvito Grasso,[e] Denise Barbut,[h] Martino Calamai,[f,i] Andrea Danani, [iD][e]
Michael Zasloff,[h,j] Annalisa Relini, [iD][d] Gabriella Caminati, [iD][c]
Michele Vendruscolo [iD][b] and Fabrizio Chiti [iD]*[a]

Trodusquemine is an aminosterol known to prevent the binding of misfolded protein oligomers to cell membranes and to reduce their toxicity in a wide range of neurodegenerative diseases. Its precise mechanism of action, however, remains unclear. To investigate this mechanism, we performed confocal microscopy, fluorescence resonance energy transfer (FRET) and nuclear magnetic resonance (NMR) measurements, which revealed a strong binding of trodusquemine to large unilamellar vesicles (LUVs) and neuroblastoma cell membranes. Then, by combining quartz crystal microbalance (QCM), fluorescence quenching and anisotropy, and molecular dynamics (MD) simulations, we found that trodusquemine localises within, and penetrates, the polar region of lipid bilayer. This binding behaviour causes a decrease of the negative charge of the bilayer, as observed through ζ potential measurements, an increment in the mechanical resistance of the bilayer, as revealed by measurements of the breakthrough force applied with AFM and ζ potential measurements at high temperature, and a rearrangement of the spatial distances between ganglioside and cholesterol molecules in the LUVs, as determined by FRET measurements. These physicochemical changes are all known to impair the interaction of misfolded oligomers with cell membranes, protecting them from their toxicity. Taken together, our results illustrate how the incorporation in cell membranes of sterol molecules modified by the addition of polyamine tails leads to the modulation of physicochemical properties of the cell membranes themselves, making them more resistant to protein aggregates associated with neurodegeneration. More generally, they suggest that therapeutic strategies can be developed to reinforce cell membranes against protein misfolded assemblies.

Introduction

Neurodegenerative disorders include a wide range of different pathologies characterized by progressive and irreversible neuronal loss, such as Alzheimer's disease (AD), Parkinson's disease (PD), amyotrophic lateral sclerosis (ALS), frontotemporal dementia (FTD), and spongiform encephalopathies (SE).[1,2] Many or most of the neurodegenerative diseases originate from the conversion of peptides or proteins from their native soluble states into fibrillar aggregates, forming various types of extracellular deposits or intracellular inclusions, including amyloid plaques, neurofibrillary tangles and Lewy bodies.[2]

Aminosterols isolated from the dogfish shark *Squalus acanthias* have been shown to act as inhibitors of amyloid formation and of the interaction of monomeric and misfolded oligomeric species with biological membranes, thus represent-

[a]Department of Experimental and Clinical Biomedical Sciences, Section of Biochemistry, University of Florence, Florence, Italy. E-mail: fabrizio.chiti@unifi.it
[b]Centre for Misfolding Diseases, Department of Chemistry, University of Cambridge, Cambridge, UK
[c]Department of Chemistry "Ugo Schiff" and CSGI, University of Florence, Sesto Fiorentino, Italy
[d]Department of Physics, University of Genoa, Genoa, Italy
[e]Dalle Molle Institute for Artificial Intelligence (IDSIA), University of Applied Sciences and Arts of Southern Switzerland (SUPSI), University of Italian Switzerland (USI), Lugano, Switzerland
[f]European Laboratory for Non-linear Spectroscopy (LENS), Sesto Fiorentino, Italy
[g]Department of Physics and Astronomy, University of Florence, Florence, Italy
[h]Enterin Inc., 2005 Market Street, Philadelphia, Pennsylvania 19103, USA
[i]National Institute of Optics, National Research Council of Italy (CNR), Florence, Italy
[j]MedStar-Georgetown Transplant Institute, Georgetown University School of Medicine, WashingtonDC, USA
†Electronic supplementary information (ESI) available. See DOI: 10.1039/d0nr05285j

ing promising drug candidates.[3–5] In this context, the most studied aminosterols have been squalamine[3] and trodusquemine (also known as MSI-1436).[4,5] Squalamine (as its phosphate salt, ENT-01) is undergoing phase-2 and phase-1 clinical trials for the treatment of PD related constipation (identifier NCT03781791) and PD related dementia (identifier NCT03938922), respectively. Trodusquemine is an equally interesting molecule because it is effective at lower doses than squalamine,[4,5] has been reported to cross the blood–brain barrier following intraperitoneal administration,[6] and can stimulate regeneration of tissues and organs following injury with no apparent effects on uninjured tissues, as observed in zebrafish and mice.[7] Recent studies in mouse models of AD demonstrated that trodusquemine can rescue spatial memory deficits, reduce plaque size and prevent neuronal loss.[8]

From a structural viewpoint, trodusquemine and squalamine are similar cationic amphipathic aminosterols (Fig. 1) as they share a sterol group, a sulphate moiety at position 24, and an alkyl polyamine group on the other side of the sterol, at position 3, consisting of a spermidine moiety in squalamine (7 methylene and 3 amino groups) and a spermine moiety in trodusquemine (10 methylene and 4 amino groups).[9,10] The additional amino group in trodusquemine results into a higher net positive charge than squalamine (+3 versus +2 at physiological pH).

Squalamine was first shown to displace from lipid vesicles monomeric α-synuclein, which is a protein associated with PD, and to inhibit its lipid-induced aggregation into fibrils.[3] It was also shown to inhibit the association of oligomers with neuronal membranes, when added to the extracellular medium, resulting in the reduction of their toxicity.[3] Finally, a transgenic *C. elegans* model of PD overexpressing human α-synuclein, and treated with squalamine, was found to be devoid of α-synuclein inclusions and to possess locomotor abilities similar to those of control worms.[3] A later report

showed that trodusquemine was also effective in inhibiting lipid-induced aggregation and secondary nucleation, while having no effect on fibril elongation, of α-synuclein.[4] Similar to squalamine, trodusquemine was also found to inhibit the association of oligomers with the membranes of cultured neurons and to prevent α-synuclein deposition and motility impairment in transgenic nematodes, but with comparable effects obtained at lower doses than squalamine.[4]

Trodusquemine was found to accelerate, rather than inhibit, the aggregation of amyloid β (Aβ), by enhancing secondary nucleation and, to a lower extent, fibril elongation, while maintaining the rate of primary nucleation unaffected.[5] These observations were also replicated *in vivo*, as *C. elegans* nematodes overexpressing human Aβ were found to form larger amounts of Aβ deposits when the medium was supplemented with trodusquemine. Given this mechanism of action *in vitro*, intriguingly, the molecule was found to rescue the motility impairment of the worms and increase their lifespan. It was also found to rescue spatial memory deficits and prevent neuronal loss in transgenic mouse models of AD.[8] Furthermore, the interaction of toxic Aβ oligomers with cell membranes and the resulting toxicity cascade was prevented by trodusquemine in neuronal cell cultures.[5] These data suggested that trodusquemine depleted the steady state population of toxic oligomers by accelerating their conversion into relatively non-toxic Aβ fibrils.[5]

However, the mechanism by which aminosterols bind to cell membranes, how they change their properties and how this process results in the displacement of misfolded protein oligomers of α-synuclein and Aβ is not yet clear. It remains in particular to be established whether trodusquemine binds to lipid bilayers. In the case of squalamine, membrane binding has been obtained only indirectly by showing that monomeric proteins, including the C-terminal domain of Na⁺/H⁺ exchanger isoform NHE3, p21-Rac1 and α-synuclein, do not bind to lipid membranes in the presence of squalamine.[3,11,12]

In this paper we focus on trodusquemine and report evidence that this aminosterol binds to the lipid bilayer of reconstituted liposomes formed by four natural lipids and to human neuroblastoma cells. Our results reveal that this binding modulates the phase domains of the lipid membranes, changing their physical properties so that the binding of misfolded protein oligomers is effectively prevented. The multidisciplinary approach in this study provides useful indications not only on the mechanism of action of this specific compound, but also about how the modulation of the physicochemical properties of lipid membranes can make them less vulnerable to the interaction and deleterious effects of misfolded protein aggregates.
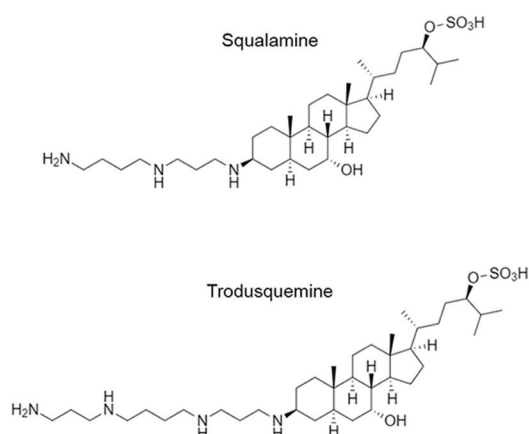

Fig. 1 Squalamine and trodusquemine structures. Comparison of the structures of squalamine (MW 628) and trodusquemine (MW 685). The two aminosterols are formed by a sulfate group (right), a sterol (centre) and a polyamine tail (left), which is a spermidine and a spermine for squalamine and trodusquemine, respectively.

Materials and methods

Preparation of large unilamellar vesicles (LUVs)

Liposomes were produced with a lipid mixture composed of 1,2-dioleoyl-*sn-glycero*-3-phosphocoline (DOPC, Avanti Polar

Lipids, Alabaster, AL, USA) and sphingomyelin (SM, Sigma-Aldrich, Darmstadt, Germany) in a molar ratio of 2 : 1 (mol/mol), 1% (mol) cholesterol (CHOL, Sigma-Aldrich) and 1% (mol) monosialotetrahexosylganglioside 1 (GM1, Avanti Polar Lipids). The lipids were dissolved in chloroform/methanol (2 : 1) and the organic solvent was removed by evaporation *in vacuo* (Univapo 150H, UniEquip, Munich, Germany) for 180 min. The mixture was hydrated at a total lipid concentration of 1 mg ml^{-1} with distilled water to form multilamellar vesicles (MLVs), left to swell for 1 h at 60 °C and then extruded 17 times through a polycarbonate membrane with 100 nm pores using a mini-extruder (Avanti Polar Lipids) at the same temperature, to form large unilamellar vesicles (LUVs). After cooling to room temperature, LUVs were stored at 4 °C for a maximum of 1 week.

Labelling of trodusquemine

Trodusquemine was synthesised as previously described and stored as a powder.[5] It was dissolved in 0.1 M sodium bicarbonate buffer, pH 7.0 to obtain a 10 mM stock solution and stored at 4 °C. BODIPY™ TMR-X NHS Ester and Alexa Fluor® 594 NHS Ester (ThermoFisher Scientific, Waltham, MA, USA) were both dissolved in anhydrous DMSO to obtain a 15 mM stock solution and stored at −20 °C. The conditions of the reaction were the same for both dyes: 5 mM trodusquemine, 0.5 mM the dye, 0.1 M sodium bicarbonate buffer, pH 7.0, in a final volume of 200 μl, at 25 °C for 1 h under mild orbital shaking. No unreacted dye was detected with mass spectrometry, whereas both unlabelled and labelled trodusquemine were detected with the expected molecular weights of 685.60 g mol^{-1} for trodusquemine alone and 1178.76 g mol^{-1} or 1308.50 g mol^{-1} for trodusquemine labelled with BODIPY™ TMR-X and Alexa Fluor® 594, respectively (Fig. S1†).

LUVs analysis by confocal microscopy

LUVs formed by DOPC/SM 2 : 1 (mol/mol) + 1% (mol) CHOL + 1% (mol) BODIPY-FL-GM1 (commercial name BODIPY-FL C5-Ganglioside GM1, ThermoFisher Scientific) were prepared at a total lipid concentration of 1.27 mg ml^{-1} and then diluted to a final lipid concentration of 0.3 mg ml^{-1} with distilled water. 100 μl of LUVs were then mixed with 200 μl of low gelling temperature agarose (Sigma-Aldrich) and mounted on a glass slide. After 5 min at room temperature the agarose was polymerised and the LUVs immobilised inside. LUVs were analysed after excitation at 488 nm using a Nikon C2 laser scanning confocal microscope (Nikon, Japan) equipped with coherent CUBE (diode 405 nm), Melles Griot (argon 488 nm) and Coherent Sapphire (Sapphire 561 nm) lasers and a Plan Fluor 100× 1.49 NA oil immersion objective. A series of 1 μm thick optical sections (1024 × 1024 pixels) was taken and analysed using the ImageJ software (NIH, Bethesda, MD, USA).

In another experiment, LUVs formed by DOPC/SM 2 : 1 (mol/mol) + 0.9375% (mol) CHOL + 0.0625% (mol) BODIPY-FL-CHOL (commercial name TopFluor® cholesterol, Avanti Polar Lipids) + 1% (mol) GM1 were made at a total lipid concentration of 1 mg ml^{-1}. 5 μM of trodusquemine labelled with Alexa Fluor 594® in a 1 : 10 (dye : trodusquemine) molar ratio was added in the swelling phase of LUV preparation. LUVs were then diluted to a final lipid and trodusquemine concentrations of 0.5 mg ml^{-1} and 2.5 μM, respectively, with distilled water. Sample preparation and confocal microscopy was then performed as described above, except that excitation was 488 and 561 nm for BODIPY-FL-CHOL and Alexa-trodusquemine, respectively.

Semi-equilibrium dialysis and NMR spectroscopy

LUVs were prepared in D_2O at a total lipid concentration of 1 mg ml^{-1} and trodusquemine, dissolved in D_2O, was added at during lipid hydration (swelling phase). 1 ml of LUVs was then dialyzed using a Float-A-Lyzer® (Sigma-Aldrich) device with a 100 kDa MWCO, in the absence and in the presence of 20 μM trodusquemine, against 3 ml D_2O for 1 h at 4 °C, to let the two solutions reach the semi-equilibrium. Three different samples were measured with NMR: the permeate deriving from LUVs with trodusquemine, the permeate deriving from LUVs without trodusquemine (negative control), and a sample of 5 μM trodusquemine in D_2O (positive control). All NMR measurements were performed at 25 °C on a Bruker 900 MHz NMR spectrometer.

Binding of trodusquemine to the cells

Human SH-SY5Y neuroblastoma cells (A.T.C.C. Manassas, VA, USA) were cultured in Dulbecco's modified Eagle's medium (DMEM, ThermoFisher Scientific), F-12 supplemented with 10% fetal bovine serum (FBS), 1 mM glutamine, and 1% penicillin/streptomycin solution. Cell cultures were maintained in a 5% CO_2 humidified atmosphere at 37 °C and grown until 90% confluence. Different concentrations (1, 2, 3, 4, and 5 μM) of trodusquemine labelled with Alexa Fluor® 594 succinimidyl ester in a 1 : 10 (dye : trodusquemine) molar ratio were added to the culture medium of cells seeded on glass coverslips for 15 min. One min before the incubation ending, the Hoechst 33342 dye was added to the culture medium (10 μg ml^{-1}). The analysis of trodusquemine-derived fluorescence and nuclei-derived fluorescence were performed after laser excitation at 561 nm and 405 nm, respectively, using the same Nikon C2 laser scanning confocal microscope and analysis method described above. All settings, including pinhole diameter, detector gain and laser power, were kept constant for each analysis.

Quartz crystal microbalance with impedance analysis (QCM-Z)

QCM experiments with impedance monitoring were carried out with a QCM-Z500 (KSV Instruments Ltd) equipped with a thermoelectric module (Oven Instruments). The resonant frequency shift (Δf) and the change in energy dissipation (ΔD) of a SiO_2 coated AT-cut 5 MHz quartz microcrystal were simultaneously measured at its resonant frequency and at the 3rd, 5th, 7th, 9th and 11th overtones (Δf and ΔD, $\Delta f_3/3$ and ΔD_3, *etc.*). The active sensor surface was 0.785 cm^2, the temperature was kept at 20 °C with a Peltier element connected to the thermoelectric module.

Naked supported lipid bilayers (SLBs) were prepared by fusion of a diluted LUVs sample (0.1 mg ml^{-1} of total lipids) in presence of 2 mM CaCl$_2$ on a SiO$_2$ quartz crystal surface.[13] The disruption process was followed monitoring Δf and ΔD and their overtones, until constant values were reached that indicated formation of a complete bilayer. Aliquots of trodusquemine solutions at 20 nM were sequentially added to the SLB-coated QCM sensor while monitoring Δf and ΔD and their overtones. The selected concentration was obtained as a surface saturation value from preliminary studies. Equilibrium adsorption on the surface was reached after 3 additions in the QCM measuring chamber.

The QCM data were analyzed by means of the commercial QCMBrowse analysis software to estimate the changes in adsorbed surface mass (Δm), surface mass density ($\Delta m/A$) and bilayer thickness employing a Voigt-based model previously used for similar systems.[14] The average surface molecular area in nm^2 per molecule was computed using

$$\text{Surface molecular area} = \left(\frac{\Delta m/A}{MW} \cdot N_A \cdot 10^{-23} \right)^{-1} \quad (1)$$

where $\Delta m/A$ is the surface mass density at adsorption saturation in ng cm^{-2}, MW is the molar mass of the adsorbed species in g mol^{-1}, N_A is the Avogadro number in molecule per mol and 10^{-23} is the unit conversion factor.

Fluorescence quenching of DPH and TMA-DPH in LUVs

1,6-Diphenyl-1,3,5-hexatriene (DPH, Sigma Aldrich) and (1-(4-trimethylammoniumphenyl)-6-phenyl-1,3,5-hexatriene *p*-toluenesulfonate) (TMA-DPH, ThermoFisher scientific) were co-dissolved with the lipid mixture in chloroform/methanol (2 : 1) to obtain a probe : lipid molar ratio of 1 : 300, and the LUVs were then obtained with the same procedure explained above. LUVs were then diluted with distilled water to 0.5 mg ml^{-1}. Increasing concentrations of trodusquemine (0 to 3.5 mM) were incubated at 25 °C for 15 min in the dark. The fluorescence spectra were acquired from 380 to 550 nm using a 3 × 3 mm black walls quartz cell at 25 °C with excitation at 355 nm on an Agilent Cary Eclipse spectrofluorimeter (Agilent Technologies, Santa Clara, CA, USA) equipped with a thermostated cell holder attached to a Agilent PCB 1500 water Peltier system. The local membrane concentration of trodusquemine that locates on the LUVs ([Q]$_m$) was calculated with

$$[Q]_m = \frac{[Q]_t}{\alpha_m} \quad (2)$$

where [Q]$_t$ is the total trodusquemine concentration, and α_m is the volume fraction of the membrane phase, corresponding to the ratio between the volume of the membrane and the water phase. The quenching of DPH and TMA-DPH was then analysed with the Stern–Volmer equation

$$\frac{F_0}{F} = 1 + [Q]_m \cdot K_{SV} \quad (3)$$

where F_0 and F are the fluorescence intensities in the absence and presence of trodusquemine, respectively; [Q]$_m$ is the local concentration of trodusquemine on the membrane and K_{SV} is the Stern–Volmer constant.

Temperature-dependent fluorescence anisotropy of DPH and TMA-DPH

LUVs labelled with DPH and TMA-DPH without and with 5 µM trodusquemine were prepared as described above, except that trodusquemine was added during the swelling phase of LUVs preparation. The fluorescence anisotropy values (r) were acquired at 430 nm in a temperature range between 20 and 50 °C with intervals of 2 °C, after excitation at 355 nm using the Agilent Cary Eclipse spectrofluorimeter described above.

Molecular dynamics simulations

A 400-lipid bilayer with the same composition of experimental LUVs (262 DOPC, 130 SM, 4 CHOL, 4 GM1 molecules) and the same bilayer with trodusquemine (2 TRO molecules) were obtained using the CHARMM-Builder,[15,16] with 3 nm of water thickness and 150 mM NaCl to neutralize the net charge system. First, 1000 steps energy minimization were conducted using the steepest descent algorithm. Two 25 ps position restrained simulations with decreasing force constants (2000 and 1000 kJ mol^{-1} nm^{-2}) were performed under the canonical ensemble at 300 K. Then, three position-restrained simulations of 50 ps (force constants of 1000, 400, 200 kJ mol^{-1} nm^{-2}) were performed using Berendsen semi-isotropic pressure coupling scheme (time step = 2 fs; pressure time constant $\tau P = 5.0$ ps)[17] at a reference pressure of 1 atm. Finally, 1 µs long production MD was carried out using the V-rescale thermostat ($T = 300$ K; $\tau T = 1.0$ ps), together with the semi-isotropic Parrinello–Rahman barostat ($P = 1$ atm, $\tau P = 2.0$ ps).[18] Two repeats of the simulations were carried out. The simulation time step was set to 2 fs in conjunction with the LINCS algorithm.[19] The particle mesh Ewald (PME) method was employed to calculate long-range electrostatic interactions.[20] The van der Waals interactions were calculated by applying a cut off distance of 12 Å and switching the potential from 10 Å. The trodusquemine protonation state was evaluated at pH 7.0 using Avogadro software.[21] The force field topology of trodusquemine molecule was taken from the CHARMM general force field.[22] The phospholipid and water topologies were parametrized by the CHARMM36m force field[23] and TIP3P model,[24] respectively. All MD simulations were performed using the GROMACS 2018 package.[25] The visual molecular dynamics (VMD) software was used to monitor all simulation trajectories.[26] The lateral diffusion coefficient (D) was obtained from the mean square displacement (MSD) of the DOPC and SM molecules, using the Einstein relation and performing a linear fitting of the MSD data over the last 300 ns. The bending modulus for monolayer (ability of the lipid membrane components to change their orientation with respect to each other), was obtained as previously described[27–29] in the last 200 ns of each MD replica, considering the DOPC and SM lipids.

DLS and ζ potential measurements

LUVs were prepared at a total lipid concentration of 1 mg ml^{-1} and trodusquemine was added during the swelling phase to reach final concentrations of 1, 4, 10, 25, 100, 250, and 500 μM. The size distribution profiles of the resulting LUVs were recorded using a Zetasizer Nano S or APS (Malvern, Worcestershire, UK) thermostated with a Peltier temperature controller and using a 10 mm reduced-volume plastic cell. The refractive index and viscosity were 1.33 and 0.89 cp, respectively. The measurements were acquired with the cell position 4.65, attenuator index 8, at 25 °C. Zeta potential (ζ) measurements were performed with a ZetaPals (Brookhaven Instruments, Holtsville, New York). About 1.6–2.0 ml of each LUV sample with and without 5 μM trodusquemine, ranging from 0.1 to 1.0 mg ml^{-1} total lipids, in 5 mM phosphate buffer, 5.57 mM ionic strength, pH 6.5, 20 °C, were added into a 4-clear faces disposable cuvette (path length 10 × 10 mm, polystyrene, Kartell™, ThermoFisher Scientific). The ζ potential values are the average of three independent thermal runs; for each temperature the ζ potential was determined as the mean of 5–10 measurements; each measurement was the average of 10 runs. We estimated the percentage error from the distribution of the relative error on the total runs for each temperature value. We found a maximum percentage error value of 3% and 5% for LUVs and trodusquemine-containing LUVs, respectively. Preliminary experiments as a function of LUVs concentration were also performed to exclude multiple scattering; the measurements were considered reliable in the 0.1–0.3 mg ml^{-1} LUV range and eventually run at 0.25 mg ml^{-1}. The electrophoretic mobility measurements were converted into ζ values according to the Smoluchowsky model.[30] The temperature was internally controlled and further monitored by means of an external probe Testo 925 AG (Testo, Lenzkirch, Germany).

Atomic force microscopy (AFM)

Supported lipid bilayers (SLBs) were obtained by depositing 40 μl of each LUV suspension (diluted to 0.1 mg ml^{-1}) and 10 μl of a 10 mM CaCl$_2$ solution onto a 1.0 × 1.0 cm^2 freshly cleaved mica substrate. The samples were stored for 10 min at room temperature and then incubated for 15 min at 60 °C in a close chamber at 100% relative humidity. The samples were cooled down at room temperature for 2 h and finally gently rinsed with Milli-Q water to remove non deposited vesicles. Prior to AFM inspection, samples were kept again at room temperature in a closed chamber at 100% relative humidity. AFM imaging usually started 1.5 h after rinsing.

Tapping mode AFM images were acquired under liquid environment using a Dimension 3100 SPM (Bruker, Karlsruhe, Germany) equipped with "G" scanning head (maximum scan size 100 μm) and driven by a Nanoscope IIIa controller (Bruker). Triangular silicon nitride cantilevers (DNP-S10, Bruker, nominal spring constant 0.06 N m^{-1}) were used. The drive frequency was 5–6 kHz and the scan rate 0.4 Hz. The heights of the L$_\beta$ domains with respect to the L$_\alpha$ phase were measured from AFM images cross sections. The values reported in the text are means ± SEM of 388 and 458 measurements in the absence and presence of trodusquemine, respectively.

Force spectroscopy measurements were performed under liquid environment with a Multimode SPM (Bruker) equipped with "E" scanning head (maximum scan size 15 μm) and driven by a Nanoscope V controller (Bruker). Triangular silicon nitride cantilevers (DNP-10, Bruker, nominal spring constant 0.24 N m^{-1}) were used. The actual spring constant of each cantilever was determined *in situ* using the thermal noise method.[31] Force maps consisting of 128 × 128 force distance curves were acquired point-by-point on scan areas of 5 × 5 μm^2 or 2.5 × 2.5 μm^2. The maximum force load was 15–18 nN. Breakthrough forces were evaluated from the force–distance curves data sets using a home-built software.

Lipid–lipid FRET

LUVs were prepared at a total lipid concentration of 1 mg ml^{-1}. Trodusquemine, when present, was added during the swelling phase to a final concentration ranging from 0 to 5 μM. BODIPY-FL C5-ganglioside GM1 (GM1-D), BODIPY-FL-cholesterol (CHOL-D), BODIPY-FL-sphingomyelin (SM-D, commercial name TopFluor® Sphingomyelin, Avanti Polar Lipids) and BODIPY-FL-DOPC (DOPC-D, commercial name TopFluor® PC, Avanti Polar Lipids) were used as donor lipids, cholesteryl 4,4-difluoro-5-(4-methoxyphenyl)-4-bora-3a,4a-diaza-s-indacene-3-undecanoate (CHOL-A, commercial name CholEsteryl BODIPY™ 542/563 C11, ThermoFisher Scientific) was used as acceptor lipid. The molar fraction of each lipid labelled with D or with A was 0.0625% of total lipids in all cases.

Fluorescence spectra of LUVs containing only lipid-D, only CHOL-A, and both lipid-D and CHOL-A were acquired on a Perkin-Elmer LS 55 spectrofluorimeter (Wellesley, MA, USA) equipped with a thermostated cell-holder attached to a Haake F8 water-bath (Karlsruhe, Germany), and on a Agilent Cary Eclipse spectrofluorimeter equipped with a thermostated cell holder attached to a Agilent PCB 1500 water Peltier system. The measurements were performed using a 3 × 3 mm black walls quartz cell at 25 °C with excitation at 450 nm and emission spectra were acquired from 480 to 640 nm. The FRET efficiency (E) was calculated as

$$E = 1 - \left(\frac{F_{\text{DA}}}{F_{\text{D}}}\right) \qquad (4)$$

where F_{DA} is the fluorescence intensity of D in the presence of A, and F_{D} is the fluorescence intensity of D in the absence of A.[32] The Förster distance (R_0) was experimentally determined from the overlap between the D emission and the A absorption using

$$R_0 = 0.211(k^2 n^{-4} Q_{\text{D}} J(\lambda))^{\frac{1}{6}} \qquad (5)$$

where k^2 is a factor describing the relative orientation in space of the transition dipoles of D and A, which is assumed to be equal to 2/3 for dynamic random averaging of D and A; n is the

refractive index of the medium, which was measured with a refractometer and it is 1.332; Q_D is the quantum yield of D in the absence of A and is 0.9 and $J(\lambda)$ is the degree of spectral overlap between the donor emission and the acceptor absorption.[32] Considering a given FRET E value calculated with eqn (4) and the R_0 value determined with eqn (5), the distance between D and A (r) was then calculated with the following equation.[32]

$$r = \sqrt[6]{\frac{R_0^6 - E \cdot R_0^6}{E}} \qquad (6)$$

Lipid-trodusquemine FRET

LUVs were prepared at a total lipid concentration of 1 mg ml^{-1} and with 5 μM trodusquemine. Trodusquemine was added in a preliminary phase of LUVs preparation, during the swelling phase. GM1-D, CHOL-D, SM-D and DOPC-D were used as donors and BODIPY™ TMR-X-trodusquemine (TRO-A) was used as acceptor. The molar fraction of each lipid labelled with D was 0.0625% of all lipids in all cases. The ratio of trodusquemine labelled and unlabelled with A was 1:10 (mol: mol). Fluorescence spectra of LUVs containing only lipid-D, only TRO-A, and both lipid-D and TRO-A were acquired on a Perkin-Elmer LS 55 spectrofluorimeter equipped with a thermostated cell-holder attached to a Haake F8 water bath, and on a Agilent Cary Eclipse spectrofluorimeter equipped with a thermostated cell holder attached to a Agilent PCB 1500 water Peltier system. The measurements were performed using a 3 × 3 mm black walls quartz cell at 25 °C with excitation at 450 nm and emission spectra were acquired from 480 to 640 nm. A negative control experiment was also carried out using lysozyme labelled with acceptor (LYSO-A) to replace TRO-A, under the same conditions. The FRET efficiency (E) was calculated applying eqn (4).

Results

Preparation and characterisation of LUVs and trodusquemine

Liposomes were prepared as large unilamellar vesicles (LUVs) at a total lipid concentration of 1 mg ml^{-1}, using DOPC and SM in a molar ratio of 2:1 (mol/mol), corresponding to 836 μM DOPC and 418 μM SM, 1% (mol) CHOL and 1% (mol) GM1, both corresponding to 13 μM each. This composition was chosen to mimic the external leaflet of neural cell membranes[33–35] and the 1% CHOL concentration, which is below the physiological level, was chosen to favour well-separated ordered domains and disordered regions.[36] LUVs were then diluted according to the requirements of the various experiments: 0.5 mg ml^{-1} for confocal microscopy, fluorescence quenching and anisotropy experiments; 1 mg ml^{-1} for NMR and FRET experiments; 0.1 mg ml^{-1} for QCM and AFM measurements; 0.25 mg ml^{-1} for ζ potential experiments. The reconstituted LUVs were found to have an apparent hydrodynamic diameter of 112.9 ± 0.7 nm and a polydispersity index (PDI) of 0.075 ± 0.004 (means ± SEM), using DLS (Fig. S2A†).

When formed with 1% (mol) GM1 uniformly labelled with BODIPY-FL, they appear as small dots of *ca.* 0.2–0.3 μm in diameter using confocal microscopy, as a consequence of the intrinsic limit of resolution of the confocal microscopy set up (Fig. S2B†). Using AFM, supported lipid bilayers (SLBs) prepared from these LUVs were found to consist of gel-phase domains (L$_\beta$ or S$_o$), with possible contributions of liquid-ordered domains (L$_o$), enriched with SM, CHOL and GM1, floating in a liquid-disordered phase (L$_\alpha$ or L$_d$, Fig. S2C†) enriched with DOPC, similarly to SLBs of similar lipid composition.[37–39] The total surface area of the L$_\beta$ domains was found to be 12.2 ± 1.3% of the total bilayer in the AFM images, corresponding to 15.4 ± 1.7% of its total mass, following the known differences in height and density between L$_\beta$ and L$_\alpha$ phases.[40] SM, GM1 and CHOL contribute, by contrast, to *ca.* 34% of our LUV mass, indicating that they are not partitioned completely in the L$_\beta$ domains, but also populate the L$_\alpha$ phase, most likely around the L$_\beta$ domains. This phase behaviour is in agreement with the finding that L$_\beta$ domains are located within larger domains that have an enrichment of the same lipids, but a height indistinguishable from the uniform L$_\alpha$ matrix.[41] Fig. S2D† reports the key parameters of the LUVs prepared under these conditions obtained using both MD simulations and experimental measurements obtained in this work (see below).

5 μM trodusquemine was added during the swelling phase of LUV preparation. Mass spectrometry indicated that trodusquemine maintained its molecular weight and did not undergo degradation when incubated under the high temperature conditions required for LUVs preparation (Fig. S1B†). LUVs were also prepared by adding 5 μM trodusquemine prelabelled with either BODIPY™ TMR-X or Alexa Fluor® 594 (probes specific for primary amines) with a molar ratio of probe:trodusquemine of 1:10, to allow its detection in confocal microscopy and FRET experiments. These labelling conditions ensured the obtainment of a trodusquemine carrying only one fluorescent dye on the terminal primary amine group of the spermine moiety (Fig. S1A†) and the absence of any unreacted probe. The mass spectrum confirmed the peaks corresponding to both labelled and unlabelled trodusquemine and no peak corresponding to the unreacted dye (Fig. S1C†).

Trodusquemine binds strongly to LUVs

LUVs containing 6.25% of CHOL labelled with the dye BODIPY-FL and 10% of trodusquemine labelled with the dye Alexa Fluor® 594 were viewed on a confocal microscope. Areas showing red fluorescence (labelled trodusquemine) also showed green fluorescence (labelled CHOL), indicating a high degree of colocalization of trodusquemine and LUVs (Fig. 2A–C), which is particularly appreciable in magnified images (Fig. 2D–F). Importantly, all dots with red fluorescence are also green, whereas red dots devoid of green fluorescence are not detectable, indicating that the whole pool of labelled trodusquemine is associated with LUVs, and that a pool of free aminosterol is absent.
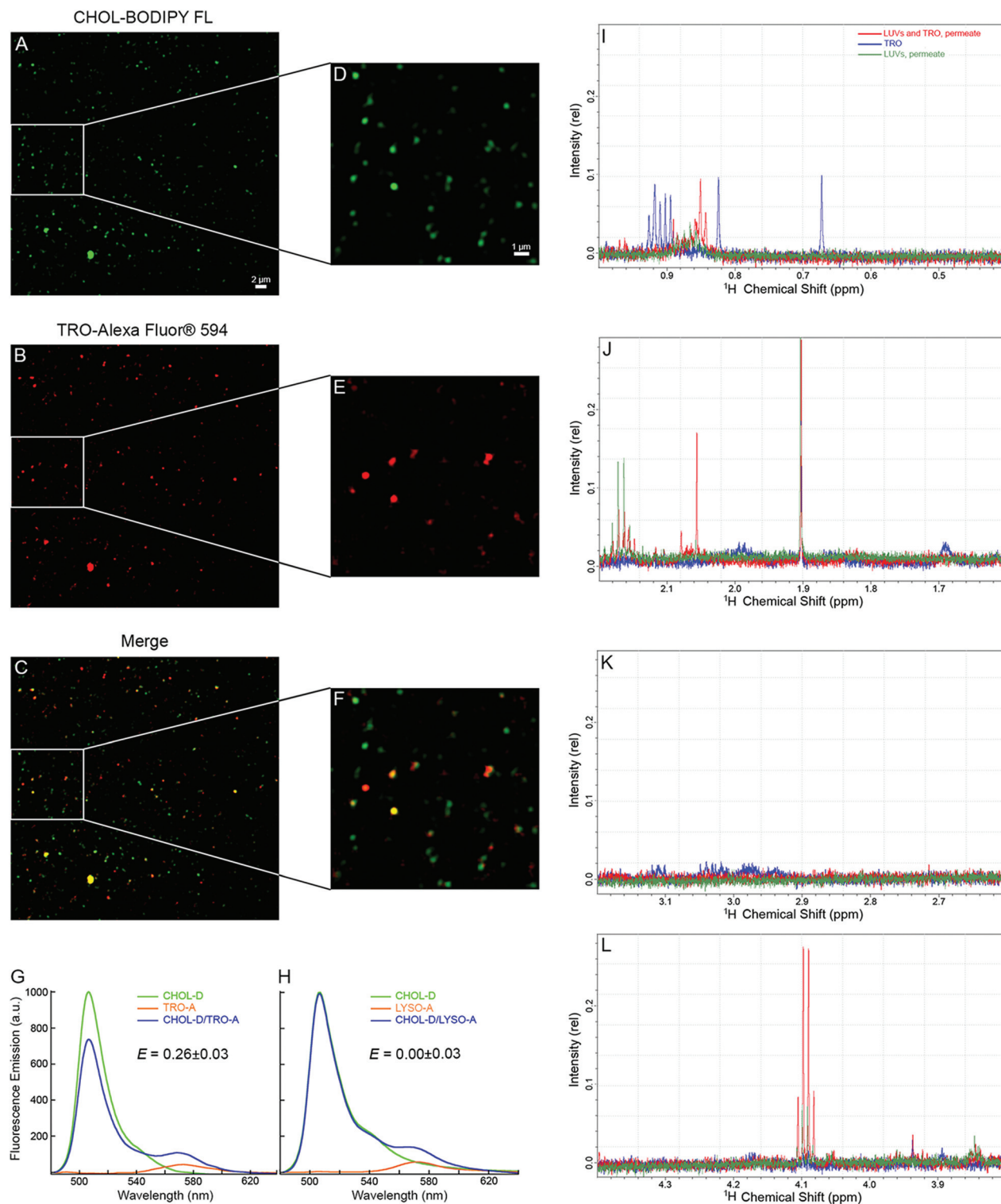
Fig. 2 Trodusquemine binds LUVs. (A–F) Representative confocal microscopy images (A–C) and corresponding magnifications (D–F), showing colocalization of trodusquemine and LUVs. Green (A and D) and red (B and E) fluorescence indicate CHOL-BODIPY-FL and trodusquemine-Alexa Fluor® 594, respectively. LUVs were formed by DOPC/SM 2 : 1 (mol/mol) + 0.9375% (mol) CHOL + 0.0625% (mol) CHOL-BODIPY-FL + 1% (mol) GM1 in the presence of 5 μM trodusquemine-Alexa Fluor® 594 in a probe : trodusquemine molar ratio of 1 : 10. (G) Fluorescence spectra recorded for the FRET experiment between LUVs containing donor-labelled CHOL (CHOL-D) and acceptor-labelled trodusquemine (TRO-A). Spectra refer to LUVs with CHOL-D (green), TRO-A (orange), both TRO-A and LUVs with CHOL-D (blue), and the arithmetic sum of CHOL-D and TRO-A spectra (violet dashed line). (H) Same as (G) but with acceptor-labelled lysozyme (LYSO-A) replacing TRO-A. The FRET efficiency (*E*) values obtained with eqn (4) (see Materials and methods) are also reported (mean ± SEM, *n* = 3). (I–L) 1D ^{1}H NMR spectra overlay deriving from the permeates of semi-equilibrium dialysis of LUVs containing trodusquemine (red), only trodusquemine (blue) and only LUVs (green).

The interaction of trodusquemine with LUVs was also investigated by fluorescence spectroscopy and FRET, using LUVs containing CHOL partially labelled (6.25%) with the donor probe (BODIPY-FL) and 5 μM trodusquemine partially labelled (10%) with the acceptor probe (BODIPY™ TMR-X). A partial energy transfer occurs from the donor-labelled CHOL to the acceptor-labelled trodusquemine (Fig. 2G), suggesting that trodusquemine is able to stably and directly interact with LUVs. As a negative control, a FRET experiment using LUVs with donor-labelled CHOL and water-soluble acceptor-labelled lysozyme, under the same conditions and using the same probes, indicated the absence of any FRET (Fig. 2H), confirming that the energy transfer observed between CHOL and trodusquemine arises from the specific binding of trodusquemine to LUVs.

In order to test whether the binding of trodusquemine to LUVs observed in the previous two experiments could depend on the presence of the fluorescent probe covalently linked to the molecule, NMR experiments were performed after a semi-equilibrium dialysis on LUVs prepared in the presence of unlabelled trodusquemine (Fig. 2I–L). In particular, 1 ml containing 1 mg ml^{-1} LUVs and 20 μM trodusquemine in D_2O were dialysed against 3 ml of pure D_2O. The 1D ^1H NMR spectrum was acquired on the permeate and compared with those obtained from 5 μM trodusquemine in the absence of LUVs (positive control) and with the permeate of a similar semi-equilibrium dialysis experiment obtained with LUVs in the absence of trodusquemine (negative control). The permeate derived from LUVs with trodusquemine did not show any of the peaks observed for the trodusquemine sample (Fig. 2I–L).

In particular, the peaks of trodusquemine at 0.67, 0.83, 0.89–0.93 (Fig. 2I), 1.69, 1.96–2.00 (Fig. 1J), 2.92–2.95, 2.96–3.00, 3.10–3.12 (Fig. 2K), 3.88 and 4.17 (Fig. 2L) ppm were not observed. These were <10% in intensity relative to those observed with 5 μM trodusquemine, leading to a dissociation constant (K_D) value <500 nM. By contrast, many of the peaks observed in the permeate derived from LUVs with trodusquemine, and not assignable to trodusquemine (Fig. 2I–L), were also observed in the permeates obtained with only LUVs or only D_2O, indicating that they originate from the dialysis membrane (data not shown). These results confirm that nearly all trodusquemine interacts with the LUVs, therefore remaining in the retentate rather than transferring to the permeate.

Trodusquemine binds to the membranes of cultured cells

Following the observation of a strong association between trodusquemine and LUVs, we extended our investigation to a cellular system. Different concentrations of trodusquemine (1, 2, 3, 4, and 5 μM) labelled with Alexa Fluor® 594 (labelled : unlabelled trodusquemine molar ratio was 1 : 10) were added to the cell culture medium of human neuroblastoma SH-SY5Y cells, and after 15 min treatment the cells were analysed by confocal microscopy. The images show the nuclei of cells stained with the Hoechst dye (Fig. 3, blue fluorescence) and trodusquemine (Fig. 3, red fluorescence) largely localising on the plasma membrane. The trodusquemine-derived fluorescence on the cell membranes progressively increases with trodusquemine concentration. Cells were also treated for the same time with the Alexa Fluor® 594 dye in the absence of trodusquemine at a concentration of 0.5 μM, corresponding to
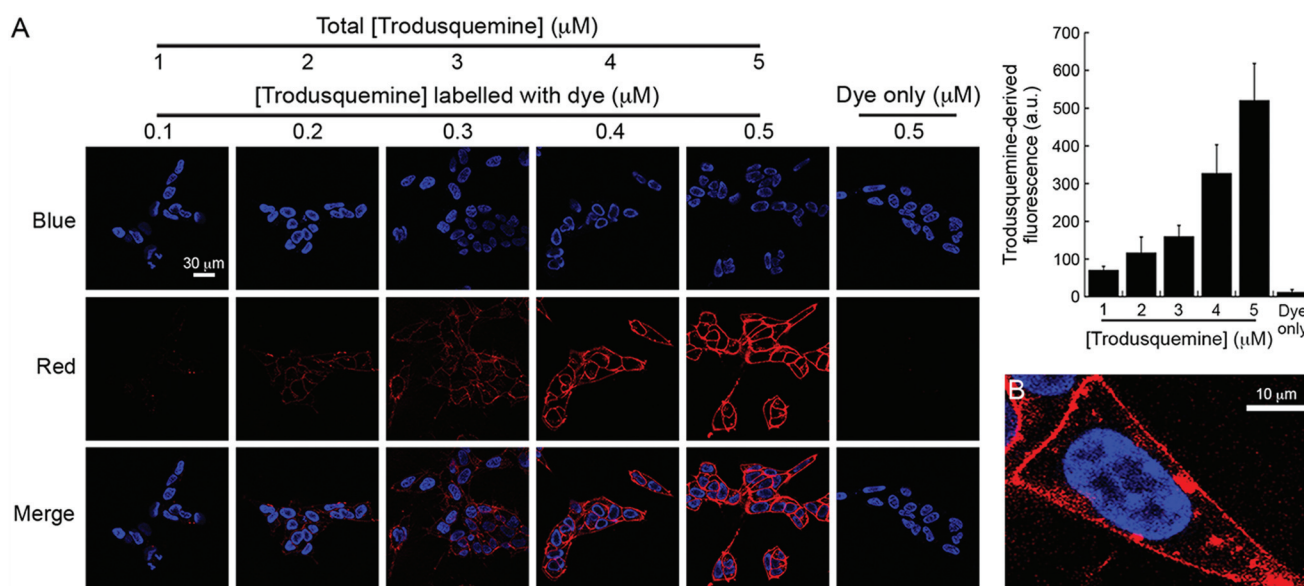

Fig. 3 Trodusquemine binds the membranes of SH-SY5Y cells. (A) Representative confocal microscopy images of SH-SY5Y cells incubated for 15 min with 1, 2, 3, 4, and 5 μM of trodusquemine labelled with Alexa Fluor® 594 (probe : trodusquemine molar ratio was 1 : 10), and with Alexa Fluor® 594 dye only at a concentration of 0.5 μM, corresponding to the dye concentration of the 5 μM trodusquemine condition. Blue and red fluorescence indicate Hoechst-labelled nuclei and labelled trodusquemine, respectively. The images were analyzed at median planes parallel to the coverslip. The histogram shows the quantitative values of trodusquemine-Alexa Fluor® 594 fluorescence. Experimental errors are SD (n = 30–35). (B) Magnified confocal image of a cell treated with 4 μM Alexa Fluor® 594-labelled trodusquemine.

the dye concentration of the 5 µM trodusquemine condition; the complete absence of dye fluorescence confirms the inability of the dye to bind *per se* to the membrane and confirms that the binding observed for the dye-labelled trodusquemine was fully attributable to the aminosterol.

Trodusquemine binds largely to the polar region of lipid bilayers

Following the observation that trodusquemine binds to the membranes of LUVs and cells, we next investigated which region of the lipid bilayer harbours the molecule. To this purpose we prepared quartz crystal microbalance (QCM) sensors coated with SLBs with the same lipid composition as the LUVs (DOPC and SM 2:1 (mol/mol), 1% CHOL and 1% GM1). Normalized changes of the third harmonic ($\Delta f_3/3$) and dissipation energy (ΔD_3) were recorded as a function of time after trodusquemine addition in the measuring chamber (Fig. 4A). Additions were repeated until a constant Δf value was obtained for all the overtones. The Δf value measured in the absence of trodusquemine was used to determine the changes in adsorbed surface mass (Δm), surface mass density ($\Delta m/A$) on the active sensor surface, bilayer thickness and mean

surface molecular area per lipid, using standard procedure of the QCM technique (Fig. 4B). The Δf value measured in the presence of trodusquemine was used to determine the changes in surface mass density ($\Delta m/A$) and bilayer thickness upon adsorption of trodusquemine on the bilayer (Fig. 4B). The surface molecular area occupied by a single trodusquemine molecule at the water-bilayer interface, obtained from the $\Delta m/A$ value at saturation according to eqn (1), was then determined, leading to a value of 94.8 ± 0.9 Å^2 (Fig. 4B). This observation suggests that the molecules are tilted on the surface with a partial insertion in the SLB, as the expected area for the adsorbed trodusquemine lying flat on the supported bilayer would be between 116 and 186 Å^2, depending on the orientation of the molecule. The experimental area of 94.8 ± 0.9 Å^2 occupied by trodusquemine led to determine an angle of *ca.* 55° for the major axis of the molecule with respect to the normal to the bilayer plane with a corresponding thickness of 14.8 ± 0.2 Å along the normal to the bilayer plane. Comparison of the observed change of bilayer thickness at the sites of trodusquemine insertion from the QCM data (5.6 ± 0.2 Å) with the expected thickness value for the tilted orientation along the normal to the SLB plane (14.8 ± 0.2 Å) suggests a partial
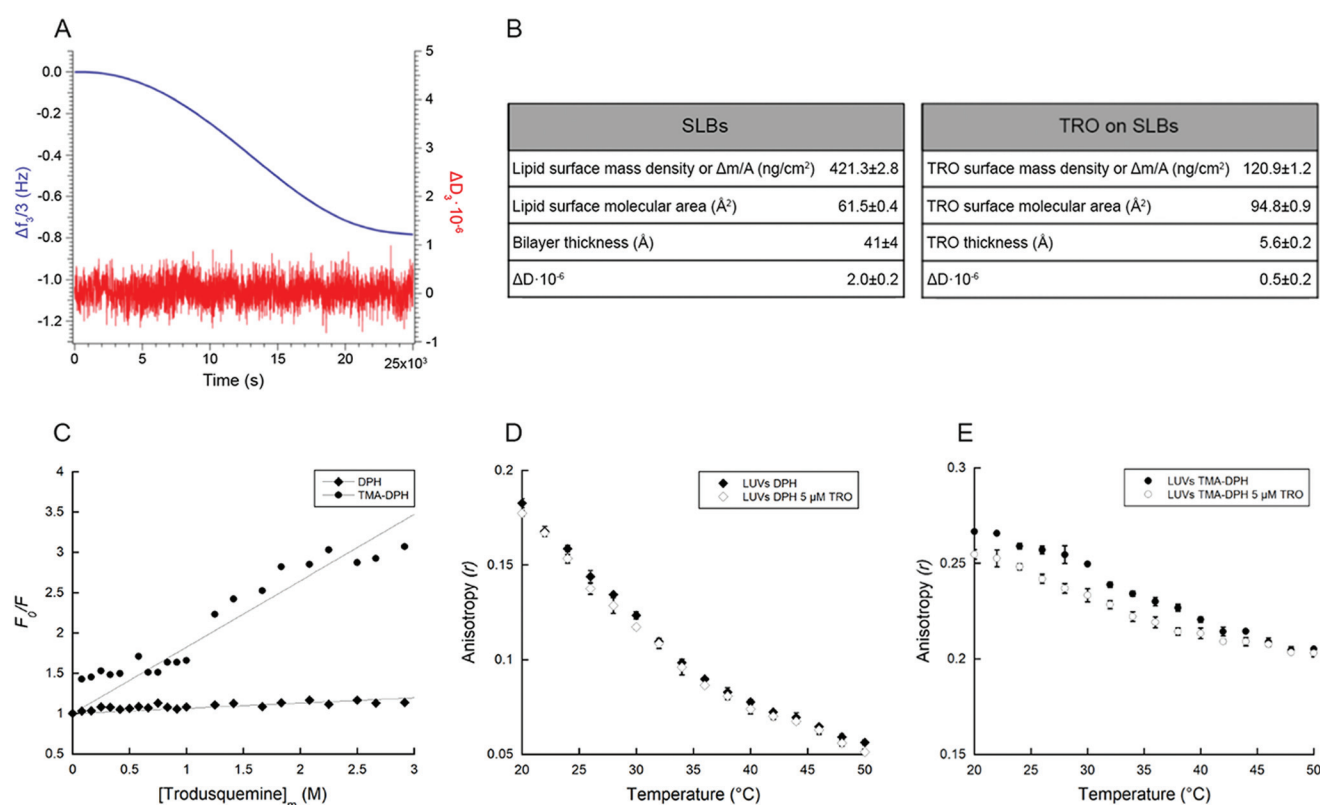

Fig. 4 Trodusquemine binds to the polar region of lipid bilayers. (A) Change in the normalized third harmonic $\Delta f_3/3$ (blue) and dissipation energy ΔD_3 (red) as a function of time after the addition of trodusquemine to the SLB-covered QCM sensor. (B) Structural and elastic properties of SLBs without trodusquemine (left) and of trodusquemine added to SLBs (right). Experimental errors are SEM. (C) Stern Volmer plot reporting the ratio of fluorescence in the absence (F_0) and presence (F) of DPH (diamonds) and TMA-DPH (circles) *versus* the membrane concentration of trodusquemine that binds to LUVs. The plots were fitted using eqn (2) and (3). (D and E) Temperature dependent fluorescence anisotropy (r) plots for DPH (D) and TMA-DPH (E), respectively, obtained in the absence (black) and presence (white) of 5 µM trodusquemine. Experimental errors are SEM of 3 different experiments.

penetration (62 ± 1.5%) of the molecule in the SLB and a partial departure (38 ± 1.5%) from the SLB plane into the solvent (Fig. 4B). The small change of ΔD_3 upon trodusquemine addition implies that the partial penetration of the molecule in the outer leaflet of the bilayer does not to affect the overall viscoelastic properties of the lipid bilayer.

The location of trodusquemine within LUVs was also studied by quenching experiments using the fluorescent probe, 1,6-diphenylhexatriene (DPH), which incorporates within the hydrophobic region of the lipid bilayer[42] and its tri-methylammonium derivative, TMA-DPH, which locates near the polar head group regions of the membrane due to its charged group.[43] The presence of trodusquemine caused a reduction of the fluorescence emission of TMA-DPH in a concentration-dependent manner, whereas it quenched DPH emission to a much lower extent (Fig. 4C). The K_{SV} constants were found to be 823 ± 33 mM^{-1} and 65 ± 6 mM^{-1}, respectively. These results indicate that trodusquemine binds nearby the polar heads of lipids rather than deeper in the hydrophobic region.

We also investigated the influence of trodusquemine on the rotational diffusion of DPH and TMA-DPH in LUVs by temperature-dependent fluorescence anisotropy. In fact, changes in the temperature-dependent fluorescence anisotropy upon trodusquemine addition reflect perturbations in the probe rotational correlation time.[44] In the absence of trodusquemine, the anisotropy of DPH and TMA-DPH was 0.183 ± 0.002 and 0.267 ± 0.001 (means ± SEM, n = 3) at 20 °C, respectively (Fig. 4D and E). This difference accounts for the lower degree of molecular packing of the lipids in the hydrophobic portion relative to the polar region, with consequent higher rotational freedom of DPH than TMA-DPH.[45] As the temperature increases, the fluorescence anisotropy decreased for both probes (Fig. 4D and E), as expected following the fluidity of the membrane lipids with increases of the rotational freedom of the two fluorophores.[45,46] Trodusquemine induced a significant decrease of the fluorescence anisotropy of TMA-DPH at all temperatures and of the temperature-dependent change of anisotropy of the same probe (Fig. 4E), whereas it had no significant effects on DPH (Fig. 4D), confirming that trodusquemine locates within the polar head region of the bilayer.

MD simulations were run to provide atomistic insights into the interaction of trodusquemine with the membrane bilayer having the same lipid composition of experimental LUVs and SLBs (2 simulations, 1 μs aggregated simulation time) and illustrated the ability of the molecule to penetrate the membrane outer layer after a few hundred ns. The small molecule, bearing a net charge of +3 (Fig. 5A), positioned at the interface between the hydrophilic and hydrophobic layers, with a solvent accessible surface area (SASA) of 40.6 ± 6.4% of the
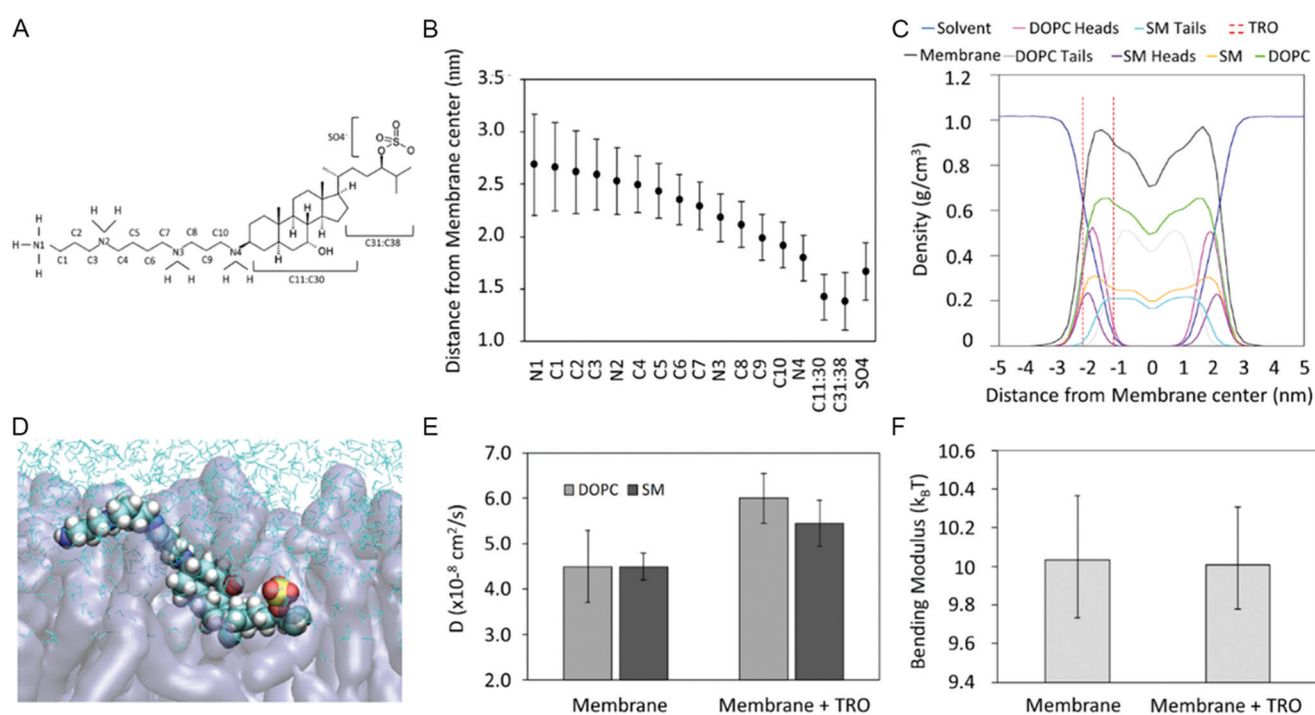

Fig. 5 Trodusquemine is partially inserted into the lipid bilayers. (A) Trodusquemine protonation state evaluated at pH 7.0 and atom numbering. (B) Distance between each heavy atom of the trodusquemine and the membrane centre of mass, evaluated during the MD simulation at the equilibrium. (C) Lipid density profile for the indicated system components along the Z coordinate (membrane centre positioned at 0.0 nm). The partial insertion of trodusquemine is indicated by red dashed lines. (D) Representative snapshot of trodusquemine within the membrane (N atoms in blue, C in cyan, H in white, O in red and S in yellow, lipids in transparent violet, water in cyan sticks). (E) Lateral diffusion coefficient (D) for DOPC and SM molecules for membrane without and with trodusquemine. (F) Monolayer bending modulus for membrane without and with trodusquemine. All experimental errors are SD.

total trodusquemine surface (Fig. 5B–D), in agreement with the experimental value of 38 ± 1.5% obtained with QCM on SLBs (see above). While the sterol ring (atoms C11 : C30) is buried into the hydrophobic domain of the membrane, the SO_4^- group and the spermine (atoms N1 : N4, C1 : C10) are in proximity of the solvent (Fig. 5A and B). However, the sulphate head is only partially in contact with the hydrophilic region of the membrane, as shown by analysing the position of trodusquemine with respect to the density profile of each system component (Fig. 5C), and also by the visual inspection of the molecular system (Fig. 5D and Movie S5†).

The impact of trodusquemine on the mechanical properties of the membrane bilayer was evaluated by computing the lateral diffusion coefficient (D) of membrane lipids and the membrane bending modulus. The D of pure membrane is 4.5 ± 0.8 × 10^{-8} cm^2 s^{-1} and 4.5 ± 0.3 × 10^{-8} cm^2 s^{-1} for the DOPC and SM lipids, respectively, in line with similar membrane composition previously investigated.[47,48] Trodusquemine increases the D value by 33% for DOPC (6.0 ± 0.6 × 10^{-8} cm^2 s^{-1}) and 21% for SM (5.5 ± 0.6 × 10^{-8} cm^2 s^{-1}), as reported in Fig. 5E. The monolayer bending modulus was found to be 10.0 ± 0.3k_BT, in accordance with previous similar composition membrane[29] and does not change upon trodusquemine addition (10.0 ± 0.3k_BT), as reported in Fig. 5F.

Trodusquemine decreases the negative charge and increases the transition temperature of LUVs

The size distributions of LUVs recorded with DLS with various concentrations of trodusquemine showed that trodusquemine, even when present at high concentrations, did not affect the monodispersity and size of LUVs (Fig. 6A and B). The zeta potential (ζ) was measured for LUVs with and without 5 μM trodusquemine. For naked LUVs at 0.25 mg ml^{-1} and 20 °C, a negative value of ζ (−23.6 ± 0.7 mV) was found and indicates a preferred exposure of the PO_4^- groups of the choline groups, as the opposite would happen if the potential were positive (Fig. 6C). This value is in agreement with literature values for DOPC- and GM1-containing liposomes.[49,50] In the presence of 5 μM trodusquemine, the ζ value was found to be −18.0 ± 0.9 mV at 20 °C, which is less negative by 5.6 ± 1.2 mV relative to LUVs in its absence (Fig. 6C). These values indicate changes in the total surface charge or changes in molecular packing of the lipid head groups induced by the presence of trodusquemine at the water-membrane interface.

Measurements of the ζ potential were then used to detect the transition temperature in the LUV systems.[51] Fig. 6C describes the behaviour of the ζ potential as a function of the temperature in the heating ramp between 10–60 °C for naked and trodusquemine-containing LUVs. Although the phase transition temperature of the present LUV system is not known, we expect the overall behaviour to be dominated by the SM component (T_m = 35–40 °C) because the most abundant DOPC lipid is already in a fluid-like phase (T_m = −17 °C) in the examined temperature range.[52,53] In the naked LUVs, we observed a sharp change in the ζ potential at $ca.$ 25 °C, supporting the dominant behaviour of SM. The ζ potential decreases with increasing temperature as usually observed for DOPC-containing lipids, reflecting a rearrangement of the surface electric dipoles packing at the interface that leads to an increase of solvent exposure of the polar groups.[54] In the trodusquemine-containing LUVs the decrease of the ζ potential starts at larger temperatures, covers a temperature range of $ca.$ 20 °C, is centred at 46 °C and is not as sharp as for the naked LUVs. These results indicate that trodusquemine interacts with the polar head groups of the LUVs, inducing a more stable molecular packing of the lipids in the bilayer.

Trodusquemine modulates the coexistence of the gel (L_β) and liquid disordered (L_α) phases

The AFM analysis of SLBs obtained by LUVs deposition on mica showed that at trodusquemine concentrations in the range 1–5 μM the coexistence of L_β and L_α phases was maintained (Fig. 7A–C), with a substantially unchanged total surface area of L_β domains (Fig. 7D). However, at 5 μM trodus-
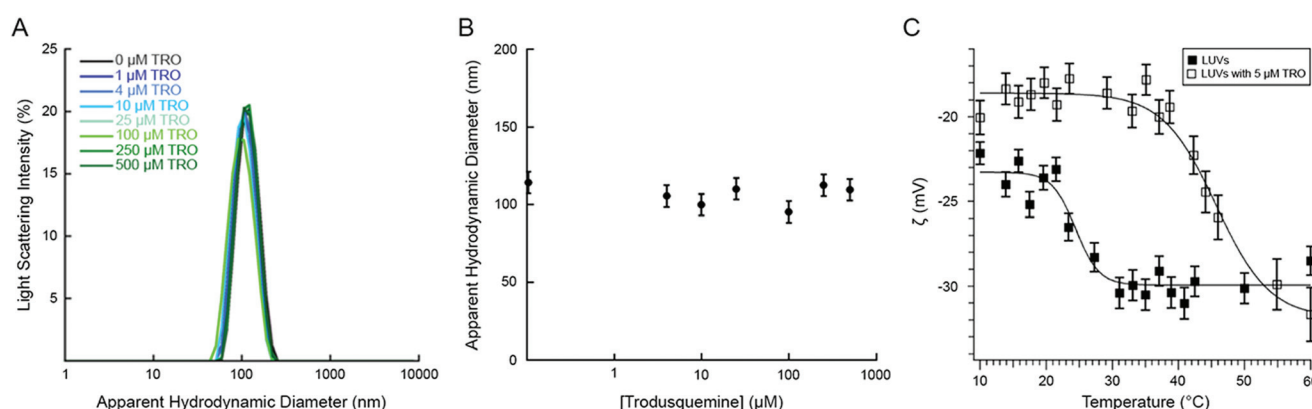

Fig. 6 Trodusquemine decreases the negative charge and increases the transition temperature of LUVs. (A) Size distributions of LUVs prepared in the presence of the indicated concentrations of trodusquemine determined with DLS. (B) Plot reporting the apparent hydrodynamic diameter *versus* trodusquemine concentration. Experimental errors are SD. (C) Zeta potential (ζ) as a function of temperature for LUVs (filled squares, ±3%) and trodusquemine-containing LUVs (empty squares, ±5%).

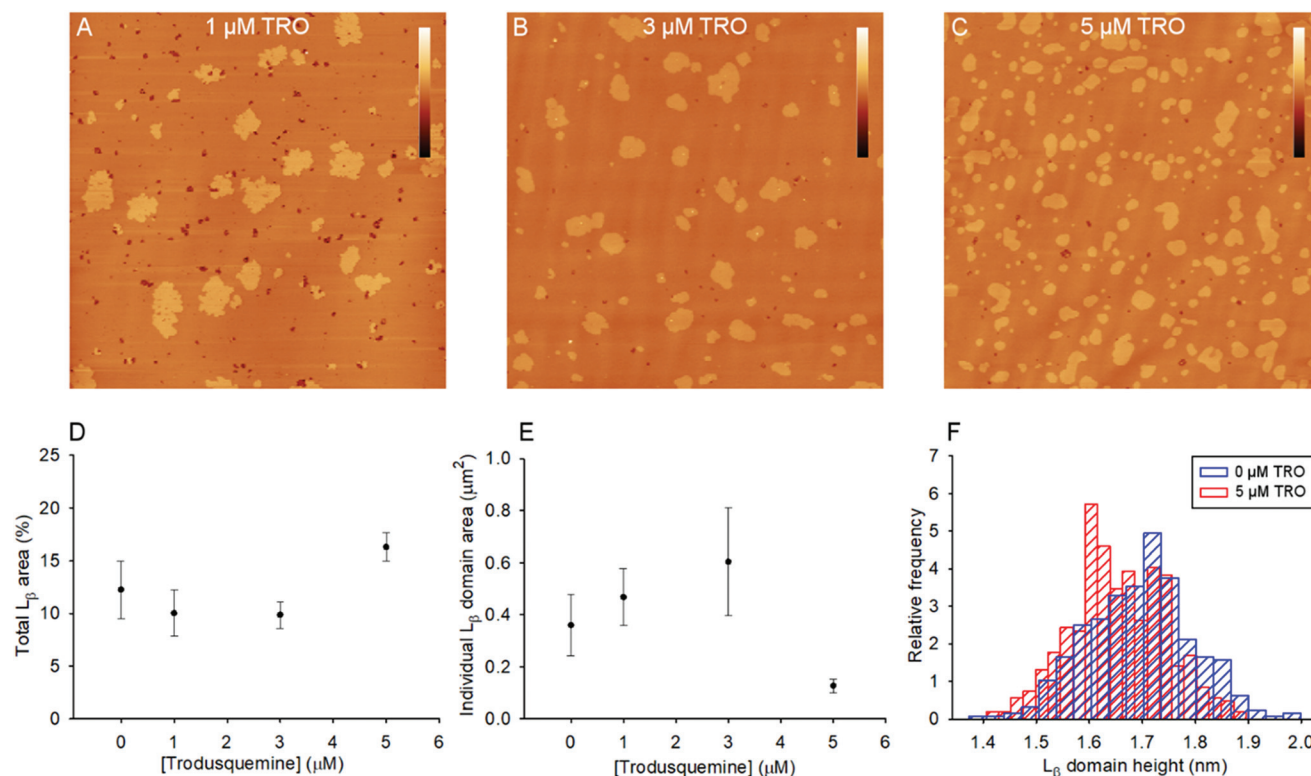**Fig. 7** Trodusquemine modulates the coexistence of the L_β and L_α phases. (A–C) AFM images (height data) of SLBs obtained from LUVs prepared in the presence of 1 μM (A), 3 μM (B), 5 μM (C) trodusquemine. The scan size is 15 μm, the color bar corresponds to a Z range of 20 nm. (D and E) Total area fraction occupied by L_β domains (D) and mean area of individual L_β domains (E), plotted as a function of trodusquemine concentration. Each point results from the analysis of at least 15 different images. Error bars were calculated with Student's statistics assuming a confidence level of 95% (2 × SEM). (F) Distributions of L_β domain height, measured with respect to the L_α phase, in the absence (blue) and presence (red) of 5 μM trodusquemine.

quemine the domains appeared to be more fragmented and the mean area per domain decreased significantly (Fig. 7E), as a consequence of the marked increase in the number of L_β domains. From the statistical analysis of the AFM image cross sections, the L_β domain height, measured with respect to the L_α phase, decreased slightly from 1.694 ± 0.005 nm (mean ± SEM, n = 388) in the absence of trodusquemine, to 1.656 ± 0.004 nm (mean ± SEM, n = 458) with 5 μM trodusquemine (Fig. 7F).

Trodusquemine induces an increase of the breakthrough force of the bilayer

AFM was also used to determine the bilayer breakthrough force, which is the force required to penetrate the bilayer with the AFM tip with a direction perpendicular to the bilayer surface. The breakthrough event corresponds to a force jump in the contact region of the approach force–distance curve and the breakthrough force is the force registered at the start of that event (Fig. 8A). We acquired force maps of the SLB surface, that is a point-by point evaluation of the bilayer breakthrough force, with each map consisting of 128 × 128 force distance curves. The force maps (Fig. 8B and C) exhibited features

which faithfully reproduced the SLB surface topography (Fig. 8E and F). L_β domains displayed higher breakthrough forces as compared with the L_α phase, but absence of breakthrough was the prevailing event for the L_β phase. Therefore, the majority of the measured breakthrough forces corresponded to L_α regions. The multi-modal distributions of breakthrough force in both conditions reflect some variability between different experiments and L_α areas, probably due to the complexity of the system under study (Fig. 8D). Nevertheless, the distribution measured with 5 μM trodusquemine is shifted towards higher force values (Fig. 8D), indicating that in the presence of trodusquemine the mechanical resistance of the bilayer to indentation is increased.

Trodusquemine clusters cholesterol molecules and separates them from GM1 in LUVs

In order to study whether or not trodusquemine affects the spatial distances between the different lipids in the LUVs, we carried out a series of lipid–lipid FRET experiments. A fraction of a given lipid type was labelled as donor with D and a fraction of CHOL was labelled as acceptor with A (Fig. S3†), so that the concentrations of D-labelled and A-labelled lipids were
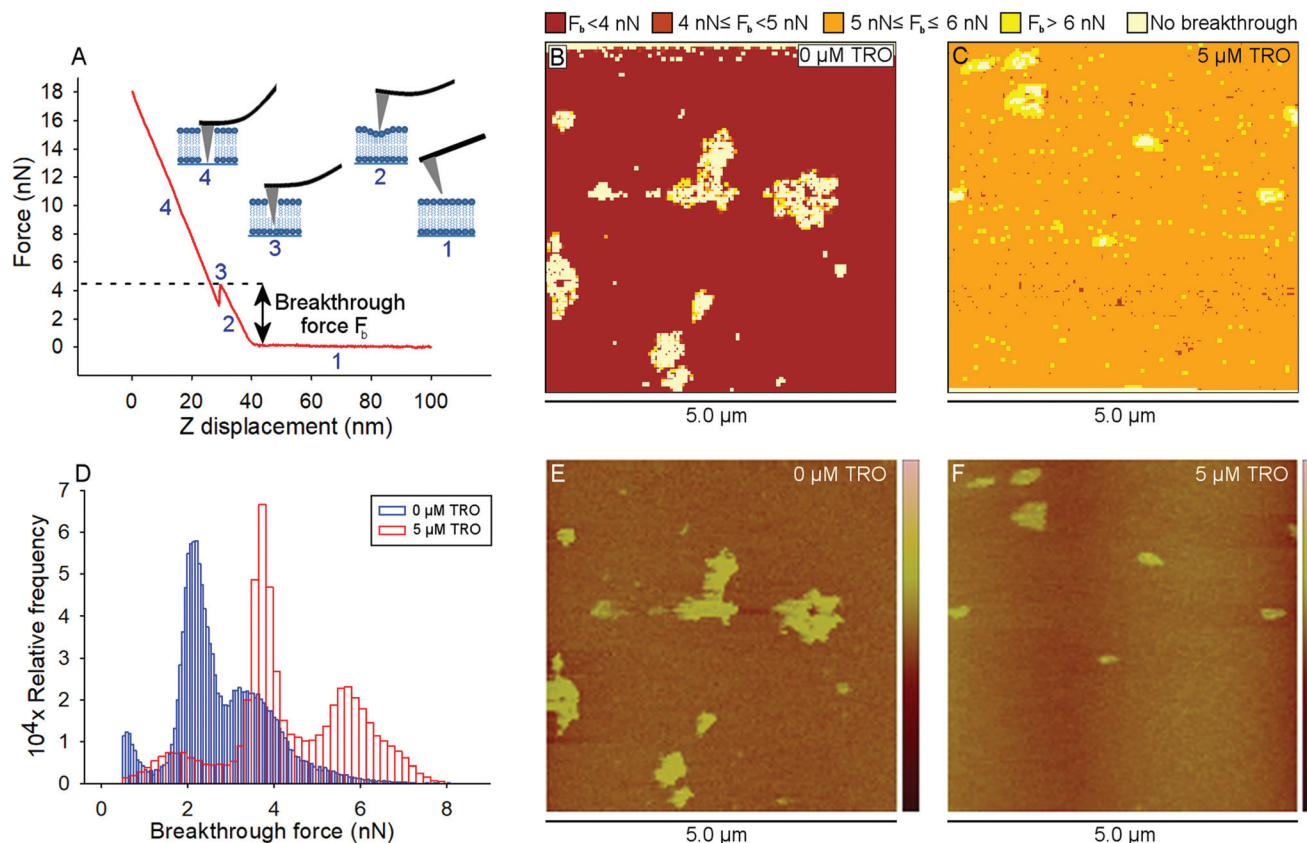
Fig. 8 Trodusquemine induces an increase of the breakthrough force of the bilayer. (A) Typical force–distance curve recorded on SLBs when the AFM tip approaches the sample surface. The force is 0 nN when the tip is distant from the bilayer (high Z displacement value, region 1 of the curve). After tip-bilayer contact, the force increases (region 2). The breakthrough force is the force value at which the tip penetrates the bilayer (point 3). Immediately after the breakthrough the force falls down, as a consequence of bilayer rupture. The force increases further because of the interaction between the tip and the solid substrate (region 4). (B, C, E and F) Breakthrough force maps (B and C) of the corresponding SLB topography images (E and F) in the absence (B and E) and presence (C and F) of 5 μM trodusquemine. The scan size is 5.0 μm and the color bar corresponds to a Z range of 15 nm (E and F). Force maps were obtained from a point-by-point determination of the breakthrough force F_b. The L_β domains usually did not exhibit breakthrough, except on their edge. (D) Bilayer breakthrough force distributions (mainly resulting from the L_α phase) in the absence (blue) and presence (red) of 5 μM trodusquemine. Distributions were obtained from five independent force maps, both with and without trodusquemine.

both 0.0625% of the total lipid concentration. The four different combinations of FRET pairs (in each case changing the D-labelled lipid type and maintaining CHOL-A) were investigated in the absence (Fig. 9A) and presence (Fig. 9B) of 5 μM trodusquemine. For each FRET pair and trodusquemine concentration, three fluorescence spectra were recorded: LUVs with both lipid-D and CHOL-A, LUVs with only lipid-D and LUVs with only CHOL-A (Fig. 9A and B). In all cases, the fluorescence emission of the D-labelled lipid was lower in the presence of CHOL-A than in its absence, and the fluorescence emission of CHOL-A was higher in the presence of lipid-D than in its absence, indicating partial FRET. In the absence of trodusquemine, the FRET E values were found to be similar for the four pairs, as expected on the grounds that three of the four lipids labelled with the donor probe studied here (SM-D, GM1-D and CHOL-D) partition equally between the L_α and L_β phases[55] and the fourth lipid that was not studied in the past (DOPC-D) occupies both the L_α and L_β even without labelling. By contrast, in the presence of 5 μM trodusquemine, an increase of E was observed in the CHOL-D/CHOL-A pair, whereas a reduction was observed in the GM1-D/CHOL-A pair (Fig. 9C–E). No significant variations were observed in the other two FRET pairs (Fig. 9C). The E value of the GM1-D/CHOL-A pair without trodusquemine was found to remain constant at different LUV concentrations spanning a ten-fold range, ruling out that the energy transfer occurs between distinct LUVs (data not shown).

For each FRET pair and trodusquemine concentration the Förster radius (R_0) was also determined and, consequently, each E value was converted into a spatial distance between D and A (r), as described in Materials and methods (Fig. 9F–H). The value of r does not represent the mean spatial distance between a given lipid and a CHOL molecule, but between lipid-D and the nearest CHOL-A (only a small fraction of both are labelled) averaged over all lipid-D molecules in the LUVs. The results show that trodusquemine induces a gradual spatial departure of GM1 from CHOL (Fig. 9G), and a progressive spatial approach of CHOL mole-
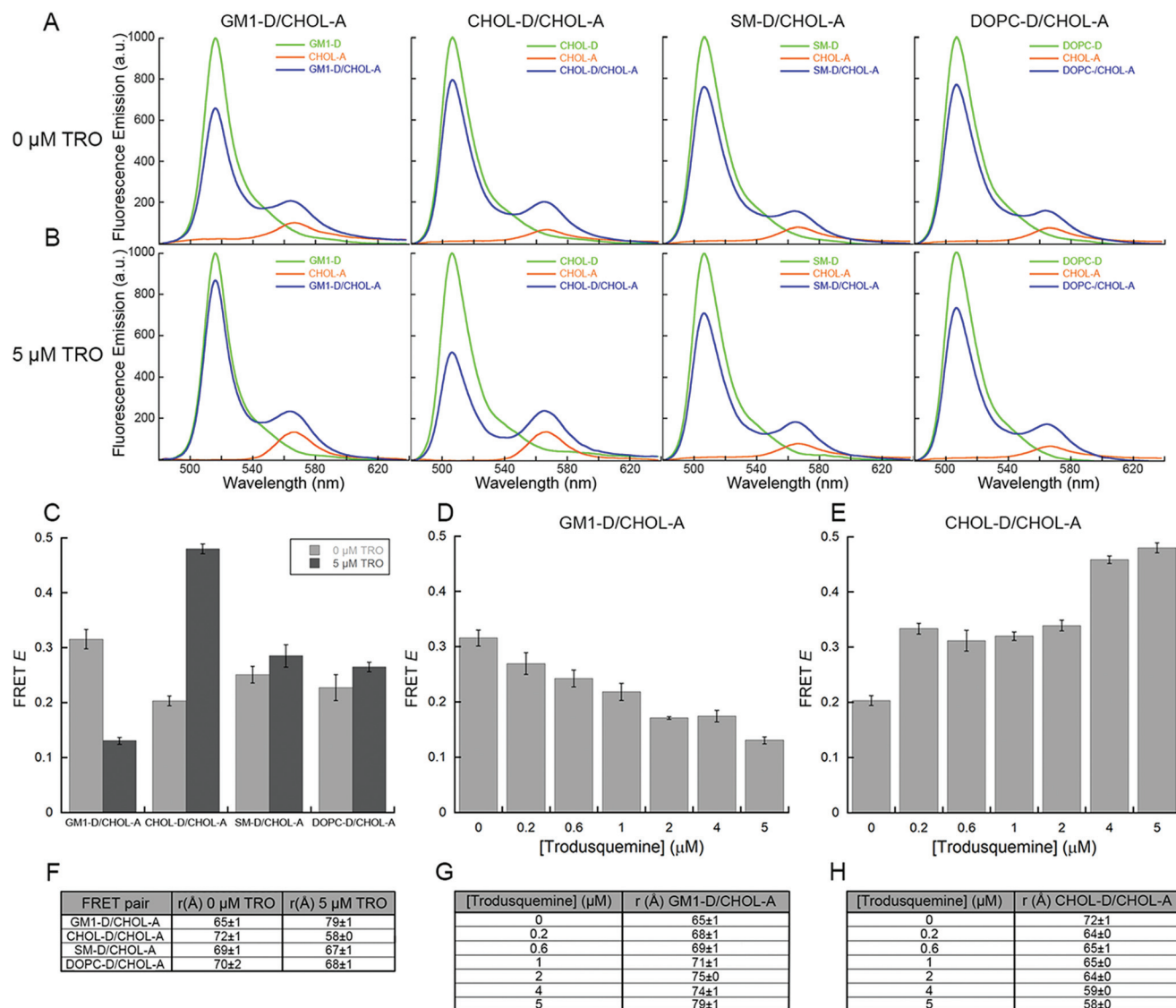
Fig. 9 Trodusquemine changes the distances between lipid molecules in the LUVs. (A) Fluorescence spectra of LUVs containing the indicated D-labelled lipid (green), A-labelled cholesterol (orange), and both (blue). (B) The same as A but in the presence of 5 μM trodusquemine. (C) FRET efficiencies (E) determined for the various pairs using eqn (4) in the absence (light grey) and presence (dark grey) of trodusquemine. (D and E) FRET efficiencies (E) of LUVs with GM1-D and CHOL-A (D) and CHOL-D and CHOL-A (E) in the presence of increasing concentrations of trodusquemine. (F–H) Spatial distances (r) between the indicated lipid-D and CHOL-A in the absence and presence of trodusquemine obtained from FRET E values reported in C–E, the R_0 values determined using eqn (5) and (6) (see Materials and methods). Experimental errors are SEM in all cases ($n = 5$).

cules in the LUVs (Fig. 9H) and, as a consequence, also between GM1 molecules.

We also found that, for both FRET pairs, r best correlated with $[TRO]^{1/2}$, rather than with $[TRO]^1$ or $[TRO]^{1/3}$, confirming that trodusquemine exerts its effects in the two-dimensions of the lipid bilayer rather than in the three-dimensions of the bulk solvent or in one-dimension (Fig. S4†).

Trodusquemine preferentially binds to the gel-phase ($L_β$) regions of the LUVs

To assess which lipids of the LUVs form preferential interactions with trodusquemine, a series of FRET experiments were carried out, where GM1, SM, CHOL, or DOPC were

labelled as donor with D (Fig. S3†) and trodusquemine was labelled as acceptor with A. The highest E value, and thus the lowest r, was found for the CHOL-D/TRO-A pair, followed by the pairs involving GM1-D, SM-D and DOPC-D, for which a FRET E value of $-0.01 ± 0.02$ was found (Fig. 10). These FRET results show that all the lipids typically enriching the $L_β$ phase determined a partial energy transfer to trodusquemine, whereas the DOPC lipid with which the $L_α$ phase is typically enriched determined a negligible transfer (Fig. 10), suggesting that the interaction of trodusquemine occurs preferentially with the lipids populating the $L_β$ phase of LUVs or nearby, where the concentrations of CHOL, GM1 and SM are still high.
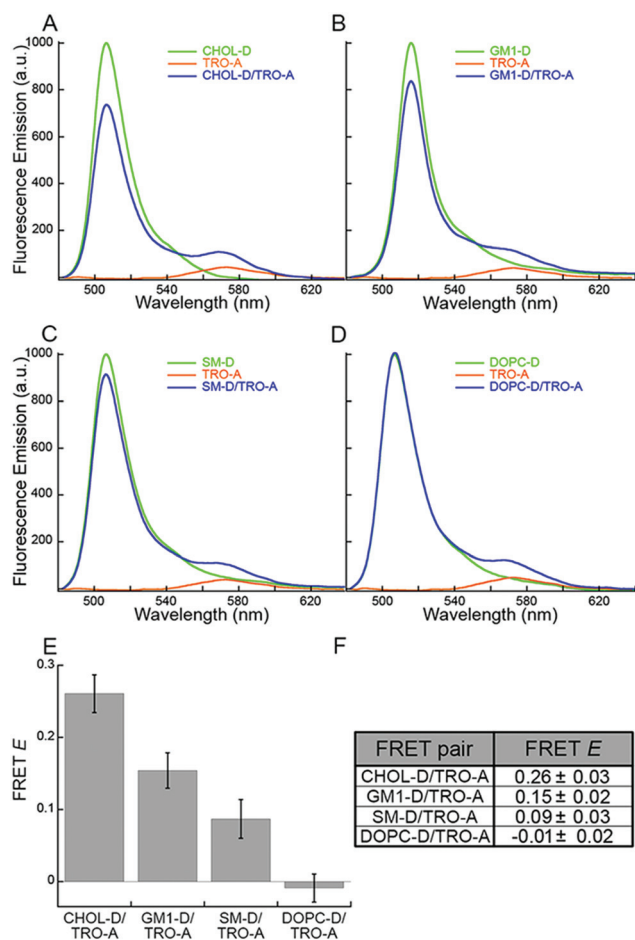
Fig. 10 Trodusquemine preferentially binds to cholesterol and GM1 within LUVs. (A–D) Fluorescence spectra of LUVs containing the indicated lipid labelled with D (green), trodusquemine labelled with A (orange) and both (blue). (E and F) Plot and table reporting the FRET E values using eqn (4). Experimental errors are S.EM in all cases (n = 3).

Discussion

Squalamine and trodusquemine have been shown to inhibit the interaction of misfolded protein oligomers with cell membranes.[3–5] The structural similarity with squalamine, its efficacy at lower doses,[4,5] its reported ability to cross the blood–brain barrier,[6] its capability to stimulate regeneration of tissues and organs,[7] and evidence of its efficacy in mouse models of AD[8] make trodusquemine an interesting candidate therapeutic molecule for neurodegenerative diseases.

In principle, the ability of trodusquemine and squalamine to prevent the binding of misfolded protein oligomers to cell membranes and to suppress their toxicity could be due to at least two non-mutually exclusive mechanisms: (i) the aminosterols bind to the oligomers preventing them from binding to cell membranes, or (ii) the aminosterols bind to cell membranes preventing them from binding the oligomers. It was recently found that trodusquemine does not affect those structural and morphological characteristics of misfolded oligo-

mers from three different protein systems that are responsible for their toxicity, when the molecule was used at a concentration of 5 μM, which is the same used in our experiments.[56] These observations do not support the first mechanism outlined above. We therefore first searched for evidence of a possible binding of trodusquemine to lipid membranes, using LUVs formed by four lipids normally found in neuronal membranes and cultured neuroblastoma cell lines. Fluorescently labelled trodusquemine was found to colocalise with fluorescently labelled LUVs in confocal microscopy and undergo FRET, as an acceptor, with one of its lipid components acting as a donor, indicating spatial proximity between trodusquemine and the lipids of LUVs. Furthermore, NMR spectra of the permeate after a semi-equilibrium dialysis on LUVs containing unlabelled trodusquemine showed a lack of trodusquemine release from the LUV membranes, indicating tight binding between trodusquemine and the LUV membranes (K_D < 500 nM), having ruled out that the binding is influenced by its covalently linked fluorescent probe. Trodusquemine-membrane binding was also observed in neuroblastoma human cells treated with labelled trodusquemine, showing a strong association of the aminosterol with plasma membranes. A similar mechanism has been found for human serum albumin, that was found, among other effects, to bind to the bilayer of LUVs preventing its interaction with αS oligomers.[57]

We then identified the regions of the membrane that harbour trodusquemine. Trodusquemine was found to partially, rather than completely, penetrate the lipid bilayer, as observed with QCM on SLBs. Moreover, it preferentially bound nearby the aqueous interface rather than deeper in the hydrophobic region, as it was able to quench and increase the rotational movement of only the fluorescent probe located in the polar head region of the bilayer. MD simulations also revealed a localisation at the interface between the hydrophilic and hydrophobic layers, with the sulphate group in proximity of the solvent and the spermine group largely exposed to the aqueous phase.

In terms of physicochemical properties of the bilayer, three major perturbations were found to occur upon trodusquemine insertion (Fig. 11). The first was a decrease of the total negative charge of the bilayer, most probably caused by the net positive charge of this aminosterol (+3 at neutral pH). Such a partial neutralisation of the negative charge of the membrane, observed with ζ potential measurements, has most likely a role in the impairment of the interaction of misfolded protein oligomers with the membranes, as this is known to be mediated mainly by GM1, in particular by its negatively charged sialic acid.[58–61]

The second major perturbation observed following the insertion of trodusquemine into the membrane was an increment of the breakthrough force applied perpendicularly to its surface, corresponding to an increased mechanical resistance of the bilayer to indentation (Fig. 11). Furthermore, an increase of the transition temperature was observed with the ζ potential measurements in LUVs containing trodusquemine, reflecting a more stable molecular packing of the lipids in the
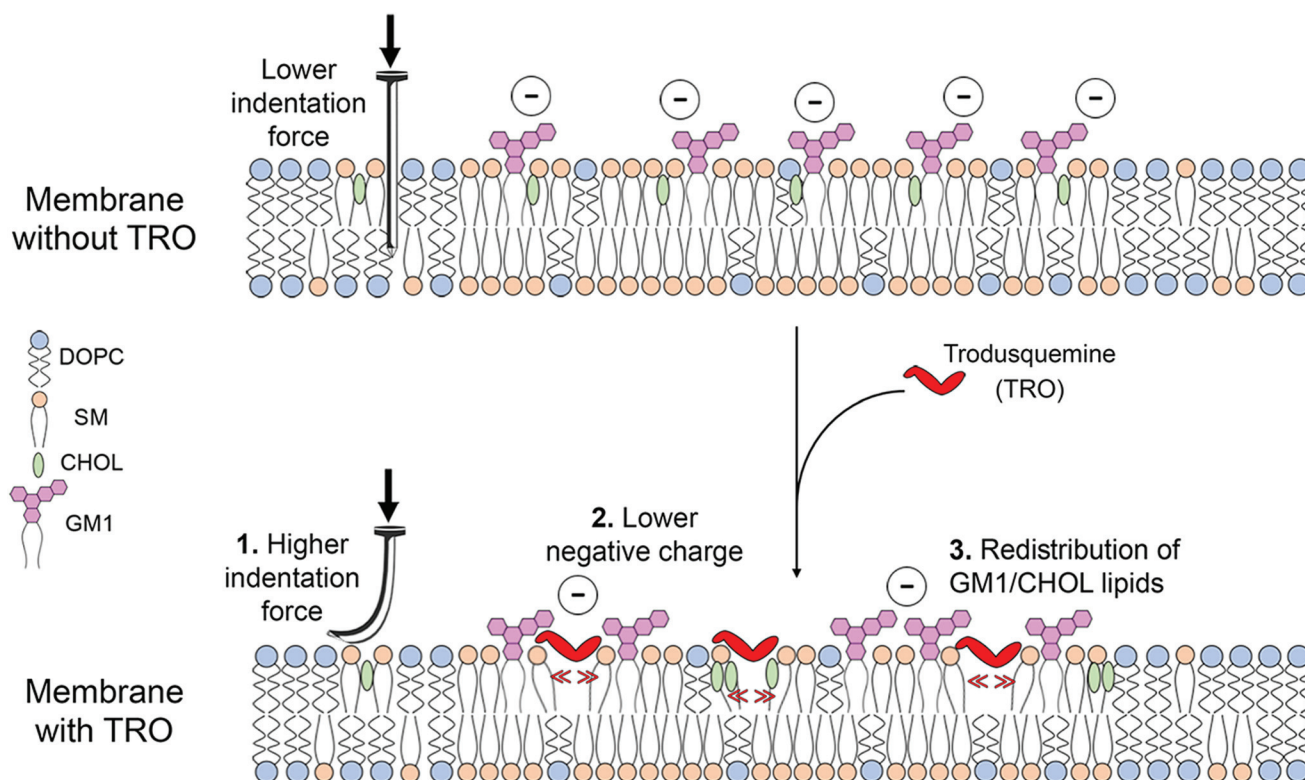
Fig. 11 Effect of trodusquemine on physicochemical properties of cell membranes linked with the toxicity of misfolded protein oligomers. Schematic representation of the three major perturbations induced by the insertion of trodusquemine in a cell membrane and thought to protect it from the disruptive action of the oligomers.

bilayer in the presence of the aminosterol. This higher stability and mechanical resistance is likely to contribute significantly to the lower vulnerability of the membranes to the action of misfolded protein oligomers in the presence of the aminosterol, as they need to penetrate into the hydrophobic portion of the bilayer to exert their toxicity.[39,62,63] Importantly, the observation obtained with AFM that trodusquemine concentrations in the range 1–5 μM do not perturb the L_α/L_β phase separation suggests that the typical trodusquemine concentrations found to be pharmacologically effective do not alter membrane properties essential for its biological function. Interestingly, in spite of an increase of the stability and mechanical resistance to indentation, the fluidity of the membrane was found to be augmented upon the addition of trodusquemine, as indicated by significant increases of the lateral translational diffusion of lipids and rotational diffusion of the TMA-DPH probe within the bilayer. The lateral diffusion of lipids is known to correlate negatively with the GM1 content and in particular with its negative charge.[64] Partial neutralisation of this excessive negative charge by the positively charged trodusquemine is likely to decrease this effect and increase lipid lateral diffusion, while creating, at the same time, an overall higher bilayer stability. In addition, the oblique insertion of trodusquemine in the membrane creates empty spaces where the lipids and TMA-DPH probe can diffuse and rotate with greater freedom. These findings indi-

cate a remarkable property of trodusquemine, which is capable to increase lipid mobility with an overall increase of the membrane mechanical properties, most probably due to its neutralising positive charge and rigidity-creating sterol group.

The third perturbation induced by trodusquemine involved the spatial distances between lipids, proportionally to its concentration, as observed with lipid–lipid FRET experiments (Fig. 11). In particular, trodusquemine increased the separation between GM1 and CHOL molecules, while forced CHOL molecules, and as a consequence also GM1 molecules, closer to one another in the surface of the lipid bilayer. Along the same lines, the aminosterol was found to interact more closely with CHOL and GM1, particularly the former, than the other two lipids, in lipid-trodusquemine FRET measurements. This finding underlines its preference for lipids forming the gel L_β phase and its ability to reorganise the spatial distribution of these two lipids that plays *per se* an important role in mediating oligomer toxicity.[65–67]

Conclusions

We have reported that trodusquemine, a natural product identified as a promising drug candidate for neurodegenerative diseases,[3–5] is incorporated into lipid membranes, particu-

larly within its superficial hydrophilic portion. Through this binding, trodusquemine modulates the physicochemical properties of the lipid membranes, even at a concentration as low as 1–5 μM, by reducing the net charge, increasing the mechanical resistance to indentation and remodelling the spatial distribution of CHOL/GM1 lipids (Fig. 11). These alterations contribute significantly to an increased resistance of the cell membranes to the toxic action of misfolded protein oligomers, thus revealing, more generally, how natural products that modulate the properties of cell membranes can protect them against the toxicity of these deleterious aggregates.

Author contributions

S.E., A.D., A.R., G.C., M.V., F.C., designed research; S.E., G.L., D.O., S.M., C.Cap., C.B., G.G., performed experiments; D.B., M.Z. contributed trodusquemine; S.E., G.L., C.Cap., C.Can., R. F., G.G., M.C., A.D., A.R., G.C. analysed data; S.E., G.L., C.C., G. G., A.R.; G.C.; M.V., F.C. wrote the paper. All authors have revised and corrected the paper.

Conflicts of interest

The authors declare the following competing interests: M.Z. is one of the inventors in a patent for the use of trodusquemine in the treatment of Parkinson's disease. M.V., is a director of Wren Therapeutics Ltd, which is independently pursuing inhibitors of protein aggregation. The remaining authors declare no competing interests.

Acknowledgements

References

1 J. Brettschneider, K. Del Tredici, V. M. Y. Lee and J. Q. Trojanowski, *Nat. Rev. Neurosci.*, 2015, **16**, 109.

2 F. Chiti and C. M. Dobson, *Annu. Rev. Biochem.*, 2017, **86**, 27.

3 M. Perni, C. Galvagnion, A. Maltsev, G. Meisl, M. B. D. Müller, P. K. Challa, J. B. Kirkegaard, P. Flagmeier, S. I. A. Cohen, R. Cascella, S. W. Chen, R. Limbocker, P. Sormanni, G. T. Heller, F. A. Aprile, N. Cremandes, C. Cecchi, F. Chiti, E. A. A. Nollen, T. P. J. Knowles, M. Vendruscolo, A. Bax, M. Zasloff and C. M. Dobson, *Proc. Natl. Acad. Sci. U. S. A.*, 2017, **114**, E1009.

4 M. Perni, P. Flagmeier, R. Limbocker, R. Cascella, F. A. Aprile, C. Galvagnion, G. T. Heller, G. Meisl, S. W. Chen, J. R. Kumita, P. K. Challa, J. B. Kirkegaard, S. I. A. Cohen, B. Mannini, D. Barbut, E. A. A. Nollen, C. Cecchi, N. Cremandes, T. P. J. Knowles, F. Chiti, M. Zasloff, M. Vendruscolo and C. M. Dobson, *ACS Chem. Biol.*, 2018, **13**, 2308.

5 R. Limbocker, S. Chia, F. S. Ruggeri, M. Perni, R. Cascella, G. T. Heller, G. Meisl, B. Mannini, J. Habchi, T. C. T. Michaels, C. K. Chala, M. Ahn, S. T. Casford, N. Fernando, C. K. Xu, N. D. Kloss, S. I. A. Cohen, J. R. Kumita, C. Cecchi, M. Zasloff, S. Linse, T. P. J. Knowles, F. Chiti, M. Vendruscolo and C. M. Dobson, *Nat. Commun.*, 2019, **10**, 225.

6 K. A. Lantz, S. G. Hart, S. L. Planey, M. F. Roitman, I. A. Ruiz-White, H. R. Wolfe and M. P. McLane, *Obesity*, 2010, **18**, 1516.

7 A. M. Smith, K. K. Maguire-Nguyen, T. A. Rando, M. Zasloff, K. B. Strange and V. P. Yin, *npj Regener. Med.*, 2017, **3**, 2.

8 K. M. Ricke, S. A. Cruz, Z. Qin, K. Farrokhi, F. Sharmin, L. Zhang, M. Zasloff, A. F. R. Stewart and H. H. Chen, *J. Neurosci.*, 2020, **40**, 1581.

9 K. S. Moore, S. Wehrli, H. Roder, M. Rogers, J. N. Forrest, D. Mc Crimmon and M. Zasloff, *Proc. Natl. Acad. Sci. U. S. A.*, 1993, **90**, 1354.

10 M. N. Rao, A. E. Shinnar, L. A. Noecker, T. L. Chao, B. Feibush, B. Snyder, I. Sharkansky, A. Sharkansky, X. Zhang, S. R. Jones, W. A. Kinney and M. Zasloff, *J. Nat. Prod.*, 2000, **63**, 631.

11 R. T. Alexander, V. Jaumouillé, T. Yeung, W. Furuya, I. Peltekova, A. Boucher, M. Zasloff, J. Orlowski and S. Grinstein, *EMBO J.*, 2011, **30**, 679.

12 M. Zasloff, A. P. Adams, B. Beckerman, A. Campbell, Z. Han, E. Luijten, I. Meza, J. Julander, A. Mishra, W. Qu, J. M. Taylor, S. C. Weaver and G. C. Wong, *Proc. Natl. Acad. Sci. U. S. A.*, 2011, **108**, 15978.

13 R. P. Richter, R. Berat and A. R. Brisson, *Langmuir*, 2006, **22**, 3497.

14 F. Gambinossi, M. Banchelli, A. Durand, D. Berti, T. Brown, G. Caminati and P. Baglioni, *J. Phys. Chem. B*, 2010, **114**, 7338.

15 J. Lee, X. Cheng, J. M. Swails, M. S. Yeom, P. K. Eastman, J. A. Lemkul, S. Wei, J. Buckner, J. C. Jeong, Y. Qi, S. Jo, V. S. Pande, D. A. Case, C. L. Brooks 3rd, A. D. MacKerell Jr., J. B. Klauda and W. Im, *J. Chem. Theory Comput.*, 2016, **12**, 405.

16 S. Kim, J. Lee, S. Jo, C. L. Brooks 3rd, H. S. Lee and W. Im, *J. Comput. Chem.*, 2017, **38**, 1879.

17 H. J. C. Berendsen, J. P. M. Postma, W. F. van Gunsteren, A. Di Nola and J. R. Haak, *J. Chem. Phys.*, 1984, **81**, 3684.

18 M. Parrinello and A. Rahman, *J. Appl. Phys.*, 1981, **52**, 7182.

19 B. Hess, H. Bekker, H. J. C. Berendsen and J. G. E. M. Fraaije, *J. Comput. Chem.*, 1997, **18**, 1463.

20 T. Darden, D. York and L. Pedersen, *J. Chem. Phys.*, 1993, **98**, 10089.

21 M. D. Hanwell, D. E. Curtis, D. C. Lonie, T. Vandermeersch, E. Zurek and G. R. Hutchison, *J. Cheminf.*, 2012, **4**, 17.

22 K. Vanommeslaeghe and A. D. MacKerell, *J. Chem. Inf. Model.*, 2012, **52**, 3144.

23 J. Huang, S. Rauscher, G. Nawrocki, T. Ran, M. Feig, B. L. de Groot, H. Grubmüller and A. D. MacKerell Jr., *Nat. Methods*, 2016, **14**, 71.

24 W. L. Jorgensen, J. Chandrasekhar, J. D. Madura and M. L. Klein, *J. Chem. Phys.*, 1983, **79**, 926.

25 M. J. Abraham, T. Murtola, R. Schulz, S. Pall, J. C. Smith, B. Hess and E. Lindahl, *SoftwareX*, 2015, **1–2**, 19.

26 W. Humphrey, A. Dalke and K. Schulten, *J. Mol. Graphics*, 1996, **14**, 33.

27 G. Grasso, S. Muscat, M. Rebella, U. Morbiducci, A. Audenino, A. Danani and M. A. Deriu, *J. Biomech.*, 2018, **73**, 137.

28 N. Johner, D. Harries and G. Khelashvili, *BMC Bioinf.*, 2016, **17**, 161.

29 G. Khelashvili, B. Kollmitzer, P. Heftberger, G. Pabst and D. Harries, *J. Chem. Theory Comput.*, 2013, **9**, 3866.

30 R. Hunter, *Zeta potential in colloid science*, Science Academic Press, 1981.

31 J. L. Hutter and J. Bechhoefer, *Rev. Sci. Instrum.*, 1993, **64**, 1868.

32 J. R. Lakowicz, *Principles of fluorescence spectroscopy*, Springer, 1983.

33 L. Pike, *Biochem. J.*, 2004, **378**, 281.

34 R. O. Calderon, B. Attema and G. H. DeVries, *J. Neurochem.*, 1995, **64**, 424.

35 H. I. Ingólfsson, M. N. Melo, F. J. van Eerden, C. Arnarez, C. A. Lopez, T. A. Wassenaar, X. Periole, A. H. de Vries, D. P. Tieleman and S. J. Marrink, *J. Am. Chem. Soc.*, 2014, **136**, 14554.

36 S. Seghezza, A. Diaspro, C. Canale and S. Dante, *Langmuir*, 2014, **30**, 13934.

37 D. Marsh, *Biochim. Biophys. Acta*, 2009, **1788**, 2114.

38 T. K. Nyholm, D. Lindroos, B. Westerlund and J. P. Slotte, *Langmuir*, 2011, **27**, 8339.

39 R. Oropesa-Nuñez, S. Seghezza, S. Dante, A. Diaspro, R. Cascella, C. Cecchi, M. Stefani, F. Chiti and C. Canale, *Oncotarget*, 2016, **7**, 44991.

40 C. Reich, M. R. Horton, B. Krause, A. P. Gast, J. O. Rädler and B. Nickel, *Biophys. J.*, 2008, **95**, 657.

41 C. Yuan, J. Furlong, P. Burgos and L. J. Johnston, *Biophys. J.*, 2002, **82**, 2526.

42 R. D. Kaiser and E. London, *Biochemistry*, 1998, **37**, 8180.

43 D. Illinger, G. Duportail, Y. Mely, N. Poirel-Morales, D. Gerard and J. G. Kuhry, *Biochim. Biophys. Acta*, 1995, **1239**, 58.

44 M. Lùcio, H. Ferreira, J. L. F. C. Lima and S. Reis, *Med. Chem.*, 2006, **2**, 447.

45 J. M. Collins, R. N. Dominey and W. M. Grogan, *J. Lipid Res.*, 1990, **31**, 261.

46 A. C. Alves, D. Ribeiro, M. Horta, J. L. F. C. Lima, C. Nunes and S. Reis, *J. R. Soc., Interface*, 2017, **14**, 133.

47 S. Chiantia, J. Ries, N. Kahya and P. Schwille, *ChemPhysChem*, 2006, **7**, 2409.

48 D. C. Carrer, A. W. Schmidt, H. J. Knölker and P. Schwille, *Langmuir*, 2008, **24**, 8807.

49 T. Al Kayal, E. Russo, L. Pieri, G. Caminati, D. Berti, M. Bucciantini, M. Stefani and P. Baglioni, *Soft Matter*, 2012, **8**, 4524.

50 E. S. Melby, A. C. Mensch, S. E. Lohse, D. Hu, G. Orr, C. J. Murphy, R. J. Hamers and J. A. Pedersen, *Environ. Sci.: Nano*, 2016, **3**, 45.

51 M. B. Sierra, V. I. Pedroni, F. E. Buffo, E. A. Disalvo and M. A. Morini, *Colloids Surf., B*, 2016, **142**, 199.

52 S. J. Attwood, Y. Choi and Z. Leonenko, *Int. J. Mol. Sci.*, 2013, **14**, 3514.

53 K. P. Shaw, N. J. Brooks, J. A. Clarke, O. Ces, J. M. Seddon and R. V. Law, *Soft Matter*, 2012, **8**, 1070.

54 M. A. Morini, M. B. Sierra, V. I. Pedroni, L. M. Alarcon, G. A. Appignanesi and E. A. Disalvo, *Colloids Surf., B*, 2015, **131**, 54.

55 E. Sezgin, I. Leventel, M. Grzybek, G. Schwarzmann, V. Mueller, A. Honigmann, V. N. Belov, C. Eggeling, U. Coskun, K. Simons and P. Schwille, *Biochim. Biophys. Acta*, 2012, **1818**, 1777.

56 R. Limbocker, B. Mannini, F. S. Ruggeri, R. Cascella, C. K. Xu, M. Perni, S. Chia, S. W. Chen, J. Habchi, A. Bigi, R. P. Kreiser, A. K. Wright, J. A. Albright, T. Kartanas, J. R. Kumita, N. Cremades, M. Zasloff, C. Cecchi, T. P. J. Knowles, F. Chiti, M. Vendruscolo and C. M. Dobson, *Commun. Biol.*, 2020, **3**, 435.

57 R. Ahmed, J. Huang, D. K. Weber, T. Gopinath, G. Veglia, M. Akimoto, A. Khondker, M. C. Rheinstädter, V. Huynh, R. G. Wylie, J. C. Bozelli Jr., R. M. Epand and G. Melacini, *J. Am. Chem. Soc.*, 2020, **142**(21), 9686.

58 J. McLaurin and A. Chakrabartty, *J. Biol. Chem.*, 1996, **271**, 26482.

59 M. Calamai and F. S. Pavone, *FEBS Lett.*, 2013, **587**, 1385.

60 S. Hong, B. L. Ostaszewski, T. Yang, T. T. O'Malley, M. Jin, K. Yanagisawa, S. Li, T. Bartels and D. J. Selkoe, *Neuron*, 2014, **82**, 308.

61 R. Cascella, E. Evangelisti, A. Bigi, M. Becatti, C. Fiorillo, M. Stefani, F. Chiti and C. Cecchi, *J. Alzheimer's Dis.*, 2017, **60**, 923.

62 G. Fusco, S. W. Chen, P. T. F. Williamson, R. Cascella, M. Perni, J. A. Jarvis, C. Cecchi, M. Vendruscolo, F. Chiti,

N. Cremades, L. Ying, C. M. Dobson and A. De Simone, *Science*, 2017, **358**, 1440.

63 R. Ahmed, M. Akcan, A. Khondker, M. C. Rheinstädter, J. C. Bozelli Jr., R. M. Epand, V. Huynh, R. G. Wylie, S. Boulton, J. Huang, C. P. Verschoor and G. Melacini, *Chem. Sci.*, 2019, **10**, 6072.

64 M. Calamai, E. Evangelisti, R. Cascella, N. Parenti, C. Cecchi, M. Stefani and F. Pavone, *Biochim. Biophys. Acta*, 2016, **1858**, 386.

65 E. Evangelisti, C. Cecchi, R. Cascella, C. Sgromo, M. Becatti, C. M. Dobson, F. Chiti and M. Stefani, *J. Cell Sci.*, 2012, **125**, 2416.

66 J. Fantini and N. Yahi, *Adv. Exp. Med. Biol.*, 2013, **991**, 15.

67 J. Habchi, S. Chia, C. Galvagnion, T. C. T. Michaels, M. M. J. Bellaiche, F. S. Ruggeri, M. Sanguanini, I. Idini, J. R. Kumita, E. Sparr, S. Linse, C. M. Dobson, T. P. J. Knowles and M. Vendruscolo, *Nat. Chem.*, 2018, **10**, 673.